Nano Research

ISSN 1998-0124 CN 11-5974/O4
https://doi.org/10.1007/s12274-019-2535-0

Research Article

A DNA origami plasmonic sensor with environment-independent read-out

Valentina Masciotti[1,2] (✉), Luca Piantanida[1,†], Denys Naumenko[1,3], Heinz Amenitsch[4], Mattia Fanetti[5], Matjaž Valant[5,6], Dongsheng Lei[7,8], Gang Ren[7], and Marco Lazzarino[1] (✉)

[1] *CNR-IOM, AREA Science Park, Basovizza Trieste I-34149, Italy*
[2] *PhD Course in Nanotechnology, University of Trieste, Trieste I-34127, Italy*
[3] *Institute for Physics of Semiconductors, National Academy of Sciences of Ukraine, Kyiv 03028, Ukraine*
[4] *Institute of Inorganic Chemistry, Graz University of Technology, Graz A-8010, Austria*
[5] *Materials Research Laboratory, University of Nova Gorica, Nova Gorica SI-5000, Slovenia*
[6] *Institute of Fundamental and Frontier Sciences, University of Electronic Science and Technology of China, Chengdu 610054, China*
[7] *The Molecular Foundry, Lawrence Berkeley National Laboratory, Berkeley CA 94720, USA*
[8] *School of Physical Science and Technology, Electron Microscopy Center of LZU, Lanzhou University, Lanzhou 730000, China*
[†] *Present address: Micron School of Materials Science & Engineering, Boise State University, Boise, ID 83725, USA*

Received: 20 June 2019 / **Revised:** 24 September 2019 / **Accepted:** 6 October 2019

ABSTRACT

DNA origami is a promising technology for its reproducibility, flexibility, scalability and biocompatibility. Among the several potential applications, DNA origami has been proposed as a tool for drug delivery and as a contrast agent, since a conformational change upon specific target interaction may be used to release a drug or produce a physical signal, respectively. However, its conformation should be robust with respect to the properties of the medium in which either the recognition or the read-out take place, such as pressure, viscosity and any other unspecific interaction other than the desired target recognition. Here we report on the read-out robustness of a tetragonal DNA-origami/gold-nanoparticle hybrid structure able to change its configuration, which is transduced in a change of its plasmonic properties, upon interaction with a specific DNA target. We investigated its response when analyzed in three different media: aqueous solution, solid support and viscous gel. We show that, once a conformational variation is produced, it remains unaffected by the subsequent physical interactions with the environment.

KEYWORDS

DNA origami, plasmonic sensor, molecular detection, gold nanoparticle

1 Introduction

Gold nanoparticles (AuNP) exhibit a peculiar opto-electronic feature commonly referred to localized surface plasmon resonance (LSPR). Surface plasmons are collective oscillations of conduction band electrons that can be excited optically by the electromagnetic radiation in presence of a periodic or aperiodic nanostructuring at a noble metal surface [1]. In case of a nanoparticle, surface plasmons are confined to the surface and are not-propagating [2]. The plasmon resonance frequency of isolated AuNP is strictly correlated with the size, the shape and the permittivity of the medium in which the colloids are embedded. When two or more AuNP are separated by less than 2.5 times the particle diameter, the mutual interaction between their plasmons results in an intensity much larger than the linear sum of the single particle plasmons and in a red-shifted frequency [3]. By exploiting this phenomenon, it is possible to create a plasmon ruler which is essentially based on the spectral shift of the scattering spectrum when two plasmonic nanoparticles approach one another. The plasmon ruler concept has been largely employed for example by coupling a metallic particle with a metallic film, demonstrating light absorptions shifts as large as 5 nm of wavelength for every 0.1 nm change in separation distance [4].

Because of their unique self-recognition properties, DNA molecules can drive the coupling of AuNP ensuring a sub-nanometric control of the interparticle distance by defining the number of nucleotides (0.34 nm each step) [5, 6], thus creating defined plasmonic field hot spots [7, 8] with a finely tuned interparticle distance. More complex DNA architectures have been realized to organize metal particles in quasi crystalline geometries with a sub-nanometric imposition of the lattice parameter [9–11] introducing further degrees of freedom in the design of their optical properties.

Due to its nearly unlimited design flexibility, DNA origami provides an unmatched platform for the realization of structures and devices at the nanoscale [12–14]. The extraordinary properties of nucleic acids of base-pair predictability, biocompatibility, mechanical strength and flexibility allow the accurate synthesis of multi-shaped objects with nanometer resolution [15]. In addition, the annealing of chemical linkers to the DNA origami structure enables the spatial addressability of numerous biological macromolecules and metal particles with nanometric precision. Thanks to its versatility, DNA origami technology was proposed for multiple applications ranging from drug delivery to quantum optics [15]. DNA nanostructures were exploited for cancer therapy by loading intercalating

Address correspondence to Valentina Masciotti, masciotti@iom.cnr.it; Marco Lazzarino, lazzarino@iom.cnr.it

chemotherapeutic agents in various DNA origami shapes. These drug carriers showed the ability to kill the tumor cells normally resistant to the chemotherapy agent used, demonstrating a good antitumor efficacy also in a mouse model for cancer [16]. Recently DNA origami technology was used for developing novel optical voltage sensing nanodevices that convert a local change of electric potential into optical signals. By using a single pair of FRET dyes, the structural changes upon application of an electric field on DNA structures reversibly immobilized on a nanocapillary tip were successfully monitored [17].

Dynamic origami structures that change conformation in response to an environmental stimulus or an external signal hold great promises in sensing and manipulation in biological environment at the nanoscale [18, 19]. The decoration of DNA origami frameworks with AuNP into fully biocompatible plasmonic DNA nanostructures offers the possibility to realize biosensors in which a biochemical event is transduced in a change in optical properties and it has been applied to enhance Raman scattering [20], fluorescence emission [21], and to develop plasmonic ruler [22, 23].

Plasmonic sensors are then extremely promising candidates for label-free single-molecule analysis not only for the compatibility with the biological environment but also for the sensitive and non-invasive detection system. Origami based plasmonic static and reconfigurable sensors sensitive to pH [24], temperature [25] and circular dichroism [26] were also proposed. However, since a biosensor can be subject to viscous forces, electrostatic forces and surface tension, it should be better independent from the surrounding environment.

In our previous paper, a continuous tuning of the LSPR was obtained localizing two AuNP respectively on the frame and on the movable part of a DNA origami hatch [27], thus resulting in an interparticle gap tuned continuously from 0 to 1.5 times the AuNP diameter. The actuation mechanism was based on DNA hybridization, in particular three different DNA sequences were shown to induce a shift in the absorption maximum wavelength of up to 6 nm. Nevertheless, when deposited on a substrate its motion and final state were strongly influenced by the electrostatic interaction with the substrate. If operated in solution, the structure design would most likely be prone to thermal fluctuations. By using a proper 3D architecture, the limitations connected to the interaction with the surrounding environment should be overcome.

A wireframe geometry benefits from high structural robustness while preserving enough flexibility to allow toggling between alternative configurations. In this paper we report the design, the synthesis, and the response of a tetrahedral DNA origami frame before and after the DNA hybridization of a specific DNA probe-target pair. The origami was actuated in aqueous solution and then its response was analyzed in three different situations: in the same solution, to simulate the operation within a body fluid, running through viscous gel, to simulate the cellular cytoplasm and other high-density physiological environments, and finally adsorbed on a silicon substrate, to emulate hard tissue, such as the core of cancer tissues or bones. For each situation we adopted the most suitable experimental approach, respectively: small angle X-ray scattering (SAXS), optical extinction and scanning electron microscopy. The device response was comparable in all conditions demonstrating a significant robustness against the influence of the external environment during the read-out process.

2 Experimental

2.1 Sensor design, synthesis and functionalization

The DNA origami structure was designed by using caDNAno software (http://cadnano.org/); design schematic is provided in Fig. S1 in the Electronic Supplementary Material (ESM); 3ss structure contained three gaps in two different pillars in which 4 nucleotide were omitted (Fig. S2 in the ESM), and the correct folding of 0ss and 3ss tetrahedrons were both verified using CanDo [28, 29] software (https://cando-dna-origami.org/). 10 nM of M13mp18 scaffold strand was mixed with staple strand mix containing 100 nM of each staple in TAE buffer (40 mM Tris, 20 mM acetic acid, 2 mM EDTA) with 12.5 mM $MgCl_2$. The mixture was subject to a cooling down ramp consisting in a rapid decrease of the temperature from 80 to 60 °C in 20 min and a slow cooling down reaching the room temperature in 40 h. Folded structures were electrophoresed in a 1% agarose gel containing TAE 1× and GelRed 1× at 50 V for 2 h. Bands were visualized with UV light and the concentration of well-folded structures were calculated with ImageJ post-processing software. AuNP were functionalized with thiol-capped oligonucleotides following a published procedure [22, 30]. Freshly prepared DNA origami structures were then incubated with ssDNA-functionalized AuNP considering a fourfold concentration of AuNP with respect to each well folded DNA origami. The annealing was favored by an incubation at 50 °C for 45 min; then the sample was slowly cooled down overnight. The anchoring success was firstly checked with agarose gel electrophoresis; the result obtained can be confirmed by the visible pink/ruby red color of the gel band matching precisely with DNA origami band detected at UV light (Fig. 1(c)). A yield of dimers formation of about 10% was obtained by evaluating DNA intensity, AuNP absorption from the gel and the results of SEM analysis as described in detail in Section 2 in the ESM.

2.2 SEM and TEM structure validation

Copper grids covered with a thin carbon layer have been activated with a plasma cleaning treatment for 5 min at 20 W (45 bias). A drop of solution is then deposited on the surface and after 5 min it is removed with a paper wiper and rinsed twice with ultrapure water. Once completely dried, it has been imaged both with SEM and TEM. The sample was first analyzed with field emission gun Supra Zeiss 40 scanning electron microscope at 2 kV of acceleration voltage, a working distance in the 2-to-5 mm range. The same sample has been then imaged with a field-emission transmission electron microscope (JEM 2100f UHR, JEOL) operated at 80 kV.

2.3 AFM analysis

AFM images have been recorded using a JPK Nanowizard II, operated in air in contact mode. AFM analysis was performed on the 2D DNA origami, deposing a 15 μL of sample in a freshly cleaved piece of mica. After 15 min of incubation, the sample was rinsed with ultrapure water and dried with nitrogen (Fig. S4 in the ESM).

2.4 Cryo-EM analysis

The specimens are prepared in standard buffered media and a drop of 4 μL is applied to an EM grid (200-mesh lacey carbon film coated grid, EMS, Hatfield, PA, and Cu-200LN, Pacific Grid-tech, San Francisco, CA). The grid is blotted for 3 s and immediately plunged into a cryogenic liquid (ethane); this step called vitrification, preventing the rearrangement of water molecule into a crystalline lattice [31]. Plunge-freezing of the cryo-EM grids has been performed using Leica EM GP (Leica, Buffalo Grove, IL) that incorporates a chamber to control the humidity (80%) and the temperature (8 °C) for blotting and thus the evaporation. The sample was stored in liquid nitrogen and remains always below −180 °C to avoid devitrification. Hydrated, unstained samples are sensitive to electron irradiation because higher doses lead to progressive alterations of molecular structures [32]. Consequently, cryo-EM images have been recorded at low electron exposures, limiting their signal-to-noise ratio (SNR).

The DNA origami architecture decorated with gold nanoparticle

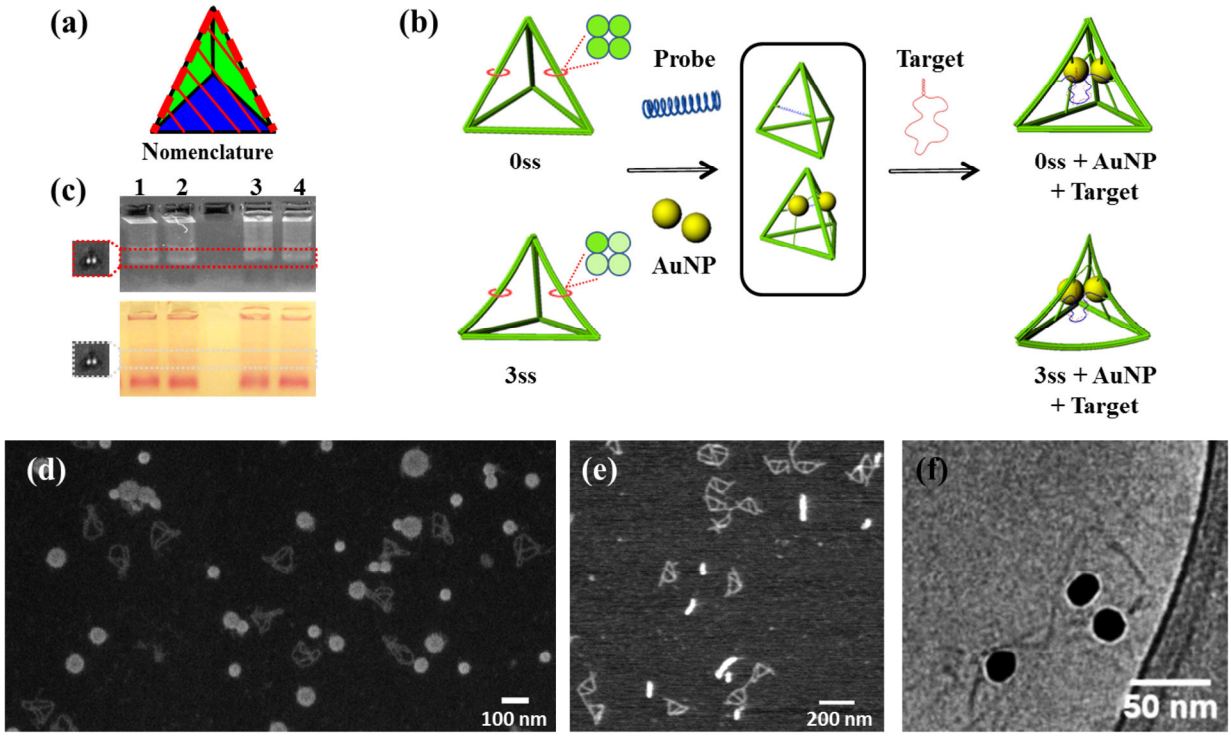

Figure 1 Design, synthesis and characterization of the tetragonal DNA origami sensor. (a) Nomenclature of the tetrahedron geometry: the blue facet is the base; the green facets are NP facets; the red striped facet is probe facet; the red dashed corners are probe struts. (b) DNA origami design: 20 nm gold nanoparticles are placed in the center of the AuNP facets so that at rest the center-to-center interparticle distance is 30 nm; a ssDNA probe links the probe struts across the probe facet. The central section of the probe struts is designed in order to have a variable flexibility. In this experiment two probe struts are used: one flexible with three single strands DNA and one double strand segment (3ss) and one with zero single strand and four double strand segments (0ss).The hybridization of a molecular target, an hairpin ssDNA strand, with the probe strand induces DNA origami squeezing, reducing the interparticle gap. (c) Agarose gel electrophoresis of 0ss and 3ss tetrahedrons decorated with AuNP before (lane 1 for 0ss, lane 3 for 3ss) and after probe-target actuation (lane 2 for 0ss and lane 4 for 3ss); the dotted boxes underline the well-folded DNA origami structures in UV/Vis mode. The excess of free staples strands is not visible in the picture because after 2 h it ran beyond the gel boundary. The AuNP band, even if coated with ssDNA, cannot be highlighted by the UV lamp because the fluorescence caused by the intercalation of GelRed requires the presence of double strand DNA. (d) SEM picture of freshly prepared DNA origami tetrahedron without AuNP on carbon TEM grid, white circles are crystallized salt residues. (e) Contact mode AFM topography in air on mica of a 2D DNA origami structures without AuNP designed and synthesized specifically to allow AFM investigations. (f) Cryo-EM image of the hybrid AuNP-DNA origami particles embedded in vitrified ice.

have been imaged with Zeiss Libra 120 transmission electron microscope (Carl Zeiss SMT GmbH, Oberkochen, Germany) under low-dose condition as descripted [33, 34]. The instrument equipped with a LaB_6 gun operating at 120 kV, an in-column energy filter, and a 4 k × 4 k Gatan UltraScan 4000 CCD camera.

2.5 SAXS measurement

AuNP-DNA origami hybrid structures were analyzed through small angle X-ray scattering (SAXS) without previous purification of the sample from excess of AuNP. SAXS data were collected with a Pilatus 1M detector (Dectris, CH) in a q-range from 0.058 to 5 nm^{-1}, at a photon energy of 8 keV [35, 36]. Sample-to-detector distance was 1,381 mm. The liquid samples were filled into flow through glass capillaries of 1.5 mm diameter (WJM-Glas /Müller GmbH, Berlin-Pankow, DE) and then measured at room temperature. Scattering data obtained were corrected for the fluctuations of the primary beam intensity and sample transmission. The background was subtracted with a corresponding buffer measurement. The conversion into 1D SAXS pattern was done with Fit2D. Data fitting analysis was performed using IGOR Pro (Wavemetrics) with custom-made functions based on the literature.

2.6 LSPR measurement

UV–vis characterization was performed using the set up described in our previous work [27]. Briefly an inverted optical microscope (Axiovert 200, Zeiss) in transmitted light illumination (HAL 100 illuminator, Zeiss) was coupled with a microscope with 750 mm long spectrometer (Shamrock SR-750, Andor Technology plc.). The distinguishable agarose gel band representing AuNP-DNA origami hybrid structures were cut out after the electrophoretic procedure and were placed onto clean glass coverslip then mounted on XY sample stage.

The light transmitted through the sample was collected by 100× immersion objective (NA 1.45, α Plan-FLUAR, Zeiss), directed into a spectrometer, split by a diffractive grating of 600 lines per mm, and finally analysed using TE-cooled EMCCD (Newton DU971-UVB, Andor Technology plc.). The extinction spectra obtained from highly concentrated AuNP were normalized using the extinction spectra of the same gel acquired in a position without AuNP.

2.7 Evaluation of the interparticle distance

A 1 × 1 cm of silicon wafer was cut and cleaned firstly with 99% ethanol and then with an oxygen plasma performed in a plasma cleaning machine applying a power of 40 W and a constant flow of oxygen for 2 min. The solution of AuNP-DNA origami was deposited on the activate substrate and incubated over there for 7 min. The excess of sample was removed through two washing steps with deionized water.

The samples were images with field emission gun Supra Zeiss 40 scanning electron microscope at the same conditions described above. The interparticle distance analysis was performed with SmartSEM® software, measuring the distance between the NP dimer from center to center to avoid AuNP dimension variability contribution.

3 Results and discussion

In order to avoid environmental effects, in the design of a structure should coexist: i) structural stability, ii) flexibility, and iii) functionality. The structure of choice was a wireframe tetrahedral DNA origami composed by six 4-helix bundles with an average length of 90 nm connected by flexible joints. A 120 bases single strand DNA probe connects two of the six struts of the structure and when hybridized with a proper target, in this case represented by a hairpin ssDNA fully complementary with the probe strand, it represents the actuator of the DNA origami device. The functionalization protocol of the 20 nm AuNP, optimized in our lab [22], consisted in the full coverage of the NP surface with thiolated ssDNA oligonucleotides. Two DNA covered-AuNP were trapped in the center of two opposite tetrahedral facets through the extension of oligonucleotides originated from the main structure. In particular each AuNP has three anchor points, or catcher strands, coming out from three different struts of a tetrahedral facet. The length of every catcher strand was accurately calculated to immobilize the AuNP in a configuration which sets the center-to-center interparticle distance to approximately 30 nm and the gap between the two surfaces to approximately 10 nm (Figs. 1(a) and 1(b)).

When the target hybridizes with the correct probe, it shortens its length and pulls toward each other the two struts on which the probe strand is anchored. As a consequence of this deformation the gap between AuNP is also reduced and the optical extinction shifted. Two different wireframes with different rigidity were designed by changing the staple strands used to fold the structures: in one case the struts that were supposed to bend upon the probe-target actuation consisted of a length-fill 4-dsDNA bundle (0ss); in the second case, 3 dsDNA were substituted with 3 ssDNA (3ss) on a 4 nucleotides-long section in the middle of the struts (Fig. 1(b), additional details of the structure in Section 1 in the ESM).

The DNA origami synthesis was validated with agarose gel electrophoresis while the formation of isolated well-folded tetrahedrons was confirmed by SEM (Fig. 1(d)) and TEM analysis (Fig. S4 in the ESM). Atomic force microscopy (AFM) was employed to confirm the structural features by analyzing the length and the diameter of the bundles which agreed with the design. Because of its 3D configuration, the tetrahedron cannot be properly imaged using AFM. By omitting six staples from the staple mix (Fig. 1(e) and Fig. S4 in the ESM), one of the six struts did not completely fold, thus obtaining a 2D origami version with a "kite-like" shape that was easily imaged by AFM.

The formation of the hybrid DNA-AuNP nanostructure was observed in the gel electrophoresis as a slower band, indicating the effective anchoring of ssDNA-functionalized AuNP to the DNA origami. DNA origami decorated with gold nanoparticles (both 0ss and 3ss) before and after the target addition, produced ruby red gel bands in the agarose gel (Fig. 1(c)). The UV light image of the same gel showing the stained DNA, provides a clear correspondence between the specific bands of the hybrid structure and the DNA origami only (Fig. 1(c)). The more intense red band in the gel is ascribed to free AuNP not bound to the DNA origami.

The proper assembly of the hybrid DNA-AuNP was finally controlled by cryo-electron microscopy (cryo-EM) [33], (Fig. 1(f), and Section 4 in the ESM) to evaluate the effective 3D structure in absence of interaction with substrates. We verified that the insertion of the AuNP does not affect the tetrahedral structure of the origami. The origami ability to recognize the target strand and, consequentially, to modify its original configuration was investigated in different environments exploiting for each of them the most suitable technique. The device behavior was analyzed using SAXS in its synthesis buffer (TAE 1× and 12.5 mM of $MgCl_2$) in the excess of free gold nanoparticles which represents a non-perturbing solution. In order to obtain high quality SAXS pattern the free AuNP were not removed since the purification due to the low yield of origami AuNP resulted in pattern with too low statistics for extracting information about the aggregation state.

The measured SAXS pattern (Fig. 2(a)) is mainly determined by the form factor scattering of the single AuNP. To investigate the differences among the working mechanism of 0ss and 3ss in aqueous solution, the structure factor of the AuNP-decorated tetrahedrons (Fig. 2(b)) was determined by dividing all traces with the free AuNP data. In this way the subtle differences among curves can be better resolved. In the following we will focus the discussion on a small portion of the plots corresponding to the $\boldsymbol{q}$ values that are expected to be affected by the interparticle distance changes. Indeed, the scattering wavevector ($\boldsymbol{q}$) is linked to the characteristic size of the sample (d_0) by the simple relation $d_0 = 2/\boldsymbol{q}$. Since a single nanoparticle (20 nm) corresponds to $\boldsymbol{q}$ = 0.31 nm^{-1} and a non-actuated dimer interparticle distance (30 nm) corresponds to $\boldsymbol{q}$ = 0.21 nm^{-1} we focused our attention on the 0.15–0.30 nm^{-1} range. For an easier comparison, Figs. 2(a) and 2(b) restricted to this range are shown in Section 5 in the ESM. The absolute value of the difference between the no target curve and the target one, shown in

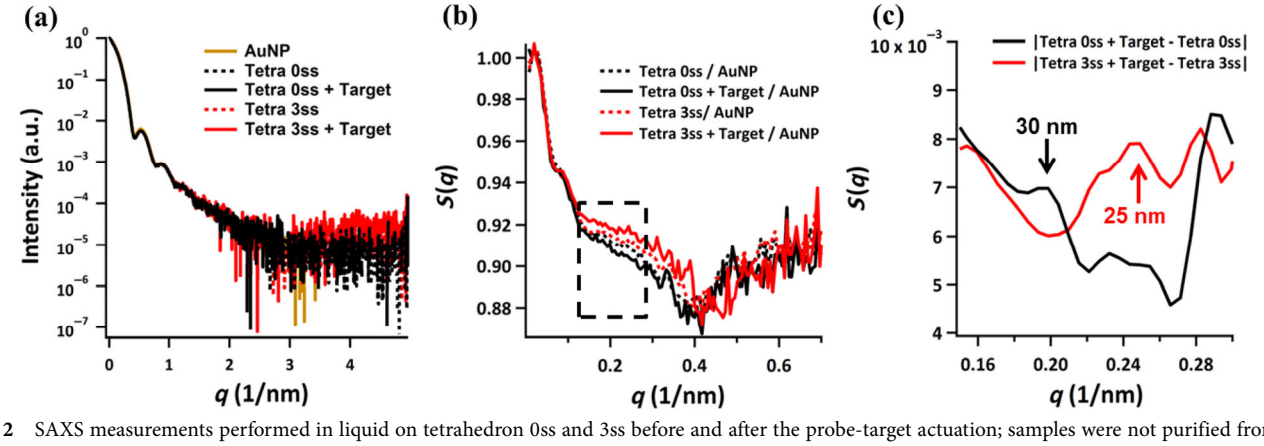

Figure 2 SAXS measurements performed in liquid on tetrahedron 0ss and 3ss before and after the probe-target actuation; samples were not purified from excess of AuNP. (a) Scattering pattern of all samples and the DNA-functionalized AuNP reference sample: all the traces mostly superimpose suggesting that the largest contribution to the signal comes from single AuNP form factor. (b) In order to extract the particle-particle interference, the structure factor has been derived by dividing the pattern with the AuNP signal (gold-yellow line). The structure factor of the different tetrahedrons highlights the presence of differences among the samples. The dashed box indicates the region of interest in which we expect to see a change in the structural factor as described in the main text. (c) The absolute value of the difference between the trace of the no target structure (dotted curves) and the traces of target structures (black and red curves) showed that the two samples are peaked at different $\boldsymbol{q}$, corresponding to different interparticle distances: 25 nm for 3ss and 30 nm for 0ss. These different peak positions demonstrate that the reduction of the interparticle distance from the initial value of 30 to 25 nm is effectively detected only with the more flexible tetrahedron.

Fig. 2(c), allows to amplify the effect of the probe-target actuation in the structure factor, where the effects of the free NP and the single loaded DNA-AuNP are suppressed. The difference pattern shows a peak at different q-values (Fig. 2(c)), corresponding to different center-to-center interparticle distances: 25 nm for 3ss and 30 nm for 0ss. These differences in the peak positions demonstrate that the reduction of the interparticle distance from the initial value of 30 to 25 nm is detected only with the more flexible tetrahedron. SAXS measurements allow also the determination of the sample clustering through the evaluation of the peak width Δq. The data in Fig. 2(c) show that the width of the peaks is reduced to 0.04 nm^{-1} in comparison to the expected value of 0.11 nm^{-1} estimated from structure factor of a double sphere model. Therefore, the signal is dominated by structures clustered as observed with cryo-EM analysis (Section 4.4 in the ESM). Nonetheless, these measurements suggest that the clustering of the AuNP tetrahedron is not affecting the working mechanism. We conclude that the designed DNA origami structures are flexible enough to be bent by the target hybridization but stiff enough to maintain the 3D configuration in aqueous environment and in presence of aggregation effects. Further analysis in liquid was performed to optically characterize the AuNP functionalized tetrahedron through sequentially measurements of the extinction spectra of aqueous solutions of AuNP with BSPP (bis(p-sulfonatophenyl)phenylphosphinedihydratedipotassium salt, used to stabilize the AuNP), DNA coated AuNP, AuNP-decorated tetrahedrons 0ss and 3ss. The normalized spectra are displayed in Fig. 3(a). The LSPR peak of DNA-covered AuNP is red-shifted with respect to AuNP in BSPP solution due to an increase of dielectric permittivity of the surrounding medium.

A further red-shift for the 0ss and the 3ss is caused by a weak plasmonic coupling between two AuNP connected to the tetrahedral DNA origami.

A larger broadening of the 3ss curve with respect to the 0ss curve can be explained by the higher flexibility of 3ss DNA origami structure leading to a less tight interparticle distance.

As for the SAXS measurements, here the contribution of free AuNP was dominating the spectra, since we did not perform any filtering or purification protocol. Moreover, it was not possible to subtract their contribution with a post processing procedure. Therefore, we did not observe the expected optical shift after the addition of the target as reported in Fig. S10 in the ESM.

To evaluate the read-out of the tetrahedral DNA origami plasmonic sensor in a viscous environment, which is a better approximation of the extracellular matrix [37, 38] and the cytosol, we purified, concentrated and then measured in agarose gel the same structure, before and after hybridization in solution [30]. Thick agarose gel may scatter light significantly, resulting in poor transmission, thus hindering UV–vis extinction measurements; therefore, the portion containing the tetrahedral DNA origami plasmonic sensor was cut to the thinnest possible section. Working with agarose gel offers an interesting advantage: running the solution through the gel it is possible to separate the different components composing the solution, and in particular, to get rid of free AuNP and DNA origami, as shown elsewhere [27].

The individual gel bands were cut out of the gel block (Fig. 1(c)) to minimize cross band contamination and the extinction spectra for each band representing 0ss and 3ss, before and after target recognition, can be acquired. The spectra before and after the target addition are shown separately for 0ss in Fig. 3(b) and for 3ss in Fig. 3(c). The two curves representing 0ss before and after target addition are peaked almost at the same position indicating that the force induced by the target is not sufficient to deform the stiffer 0ss frame, as already observed in water. On the contrary, on the 3ss tetrahedron the target triggers a consistent (8 nm) red-shift in the optical response (Fig. 3(c)): as already observed with SAXS measurements, the weakened struts are flexible enough to be deformed upon target recognition; moreover, such deformation is not further modified by the increased viscosity of the read-out medium and remains consistent with SAXS measurements.

We used Mie theory [1, 39–41] in order to evaluate the interparticle gap change in the 3ss DNA origami tetrahedron before and after target addition. First, we obtained the value of the effective dielectric permittivity ε_{eff} of DNA coated AuNP in water; this value was corrected in gel (see Section 6.2 in the ESM for more details) to calculate the AuNP surface-to-surface distance in gel network. The obtained values are 9.2 and 5.4 nm for no target and target 3ss tetrahedrons, respectively, which correspond to 29.2 and 25.4 nm of center-to-center interparticle distance, thus reproducing, also numerically, the SAXS results.

The effect of the interaction with a rigid substrate has been successively studied. A small droplet of solution containing the tetrahedral DNA origami-AuNP hybrid structures before and after target addition were incubated on clean silicon substrate that had been previously treated with 2 min oxygen plasma. After 7 min of incubation, the samples were washed twice with MilliQ water and let dry, so that it was possible to image the origami structures with scanning electron microscope (SEM). SEM imaging enables not only the visualization but also the calculation of the center-to-center interparticle distance by analyzing the brightness profile of the images. Its statistical distribution, calculated measuring the interparticle distance of 96 structures for 3ss before (black) and 69 structures for 3ss after (red) the target hybridization, is shown in Fig. 4(a). Before hybridization the distribution is broad and bimodal, peaked at 27 and 33 nm. Indeed, the flexible 3ss structure

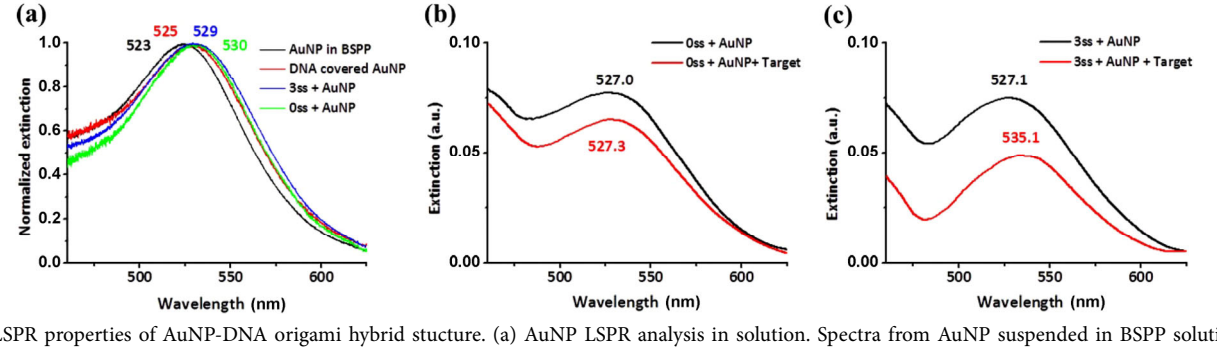

Figure 3 LSPR properties of AuNP-DNA origami hybrid stucture. (a) AuNP LSPR analysis in solution. Spectra from AuNP suspended in BSPP solution (black), DNA coated AuNP (red), 0ss (green) and 3ss (blue) origami are displayed. The LSPR peak of DNA-covered AuNP is red-shifted with respect to AuNP in BSPP solution due to an increase of dielectric permittivity of the surrounding medium. A further red-shift for the 0ss and the 3ss is caused by a weak plasmonic coupling between two AuNP connected to the tetrahedral DNA origami. A larger broadening of the 3ss curve with respect to the 0ss curve can be explained by the higher flexibility of 3ss DNA origami structure leading to a less tight interparticle distance. (b) AuNP LSPR analysis in agarose gel, after purification. Spectra from 0ss structures with (red) and without (black) target. No spectral shift is observed. (c) AuNP LSPR analysis in agarose gel, after purification. Spectra from 3ss structures with (red) and without (black) target. A significant red-shift is observed attributed to the interparticle distance reduction due to the probe-target hybridization.

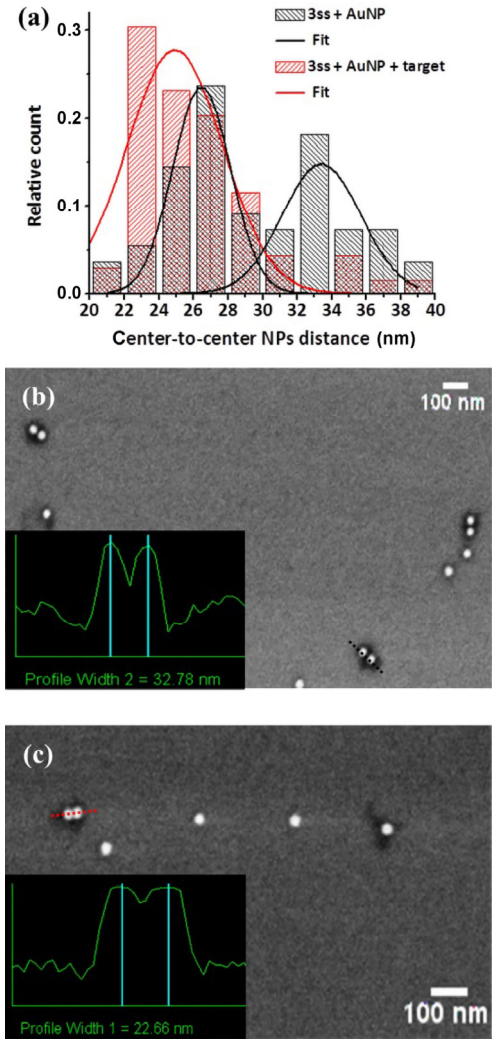

Figure 4 SEM analysis of the interparticle distance. (a) Statistical distribution of interparticle distance (center-to-center) of 3ss dimers before (black) and after (red) the hybridization of target. The interparticle gaps were evaluated measuring the brightness profile of the SEM pictures through SEM SUPRA software tool. Before hybridization the distribution is broad with a bimodal character peaked at 27 and 33 nm. After target hybridization, the distribution become monomodal peaked at 23–24 nm. (b) and (c) Representative SEM image of not purified DNA origami samples. Well-folded 3ss tetrahedron decorated with two gold nanoparticles are easily identified and distinguishable from the free AuNP also present in the solution. In the inset a representative profile used to evaluate the interparticle gap of 3ss before (b) and after (c) probe-target actuation.

toggles between a broad range of configurations, ranging from the AuNP contact to a separation of 20 nm, peaked around its equilibrium configuration of 30 nm. The four facets of the tetrahedral structures have the same probability to get in contact to the silicon solid surface, but the two surfaces with the AuNP have a much smaller contact area and thus a lower sticking probability. Moreover, in this case the two AuNP would appear superimposed in the SEM image and they would not be considered in the statistics. If the facet containing the probe is interacting with the substrate, the electrostatic interaction will freeze it in the configuration it had last assumed while in solution, which in absence of a probe-target interaction is the one with the largest AuNP distance (33 nm). On the other hand, the docking of the fourth facet exposes the flexible parts to the capillary forces developed during drying which shrinks the structure to an interparticle distance of 27 nm. The docking of these two facets has similar probability, hence the bimodal distribution. When the target hybridizes before the docking, the distribution becomes monomodal and peaked at 25 nm. The addition of the target pulls the struts closer and stiffens the whole structure in a shrunk configuration, independently from the facet docking, and in agreement with the LSPR and SAXS analysis. These data show that the interaction with a solid surface after hybridization does not influence the configuration, which depends only on the presence of the target.

These results together demonstrate that the designed 3ss tetrahedron maintains the structural modification induced by target hybridization irrespective of the environment in which it is measured: aqueous solution, highly viscous matrix, deposited and dried on a solid substrate. In particular, 3ss tetrahedron shows the capability to switch its configuration by reducing the interparticle gap in a controlled way, without being clearly perturbed by capillarity, viscosity, adhesion forces and surrounding pressure. It can still be slightly affected by thermal fluctuations in aqueous solution, as shown in LSPR analysis in graph in Fig. 3(a), where the 3ss shows a wider peak than the 0ss. The 0ss instead does not change its configuration, thus highlighting the higher rigidity of the "fully double strand" structure, which hinders the proper response when stimulated by the target. In addition, the plasmonic properties of the sensor could promote the fast and non-invasive LSPR detection of numerous targets of medical interest not only *in vitro* but also *in vivo*, improving the actual diagnostic in term of target localization and clinical invasiveness.

4 Conclusions

In this work we described a DNA origami-based plasmonic device in which a biomolecular reaction produces a structural reconfiguration. The device has a tetrahedral structure with rigid struts connected by flexible joints. To increase its flexibility, in one design, we introduced 4-nucleotides gaps in three helices of the bundle positioned in a specular way in the two struts connected by the actuator strand. The detection strategy relies on the plasmonic response of two AuNP strategically positioned on two opposite facets of the tetrahedron: any relevant structural change, which may result in a nanometric change of the interparticle gap, can be monitored through extinction measurements. The actuation, triggered by the hybridization with a molecular target, induces a clearly detectable red-shift of the peak position of AuNP LSPR spectrum proportional to the interparticle distance reduction. The optical extinction measurements of target hybridized and not hybridized structures highlighted the presence of an LSPR shift in the target hybridized 3ss samples only, confirmed by in-depth analysis of conformational changes performed using SAXS detection. We investigated the effect of the environment in which the switch of the configuration is evaluated, by performing SAXS measurements in aqueous environment, LSPR measurements in a highly viscous agar gel matrix and SEM imaging with the DNA origami tetrahedron interacting with a solid substrate, and in all environments a consistent gap reduction between AuNP after the probe-target recognition was observed. The tetrahedral DNA origami has demonstrated the environment independence for which it has been originally designed, paving the way to its application in the field of molecular recognition in different conditions. Moreover, its biocompatibility due to both its tetrahedral shape, compatible with most cell uptake mechanisms [42, 43], and its material, DNA and AuNP, suggests that the wireframe tetrahedron presented in this paper could be taken in consideration for *in vivo* analysis, for example as an injectable biosensor or as a contrast medium for biomarker detection. The new technology is not restricted only to the recognition of DNA targets. The substitution of the DNA probe with antibodies and aptamers would allow the detection of antigens or protein markers both *in vitro* and *in vivo*, enabling the target diagnosis directly in the native environment.

5 Materials

Unless otherwise specified, chemicals and reagents were purchased from Sigma-Aldrich. The oligonucleotides custom design for the folding of the tetrahedral structure with an average length of 32 nts and the 3′ thiol-capped DNA oligonucleotides for the AuNP coverage were purchased with HPLC purification from Sigma-Aldrich. M13mp18 is a M13 lac phage vector long 7249 nts (250 μg/mL) and was purchased from New England BioLabs Inc. GelRed™ DNA staining solution was purchased from Biotium. Gold colloids (AuNP), 20 nm in diameter with a coefficient of variation < 8% supplied in water, and Muscovite Mica grade V1 were purchased from Ted Pella, Inc. AFM imaging was performed using Olympus OMCL-TR400PSA AFM tips with a pyramidal tip (spring constant 0.02–0.08 N/m).

Acknowledgements

V. M. acknowledges financial support from MIUR (MIUR Giovani-Ambito "Salute dell'uomo"). Work at the Molecular Foundry, under the research project No. 3376, was supported by the Office of Science, Office of Basic Energy Sciences, of the U.S. Department of Energy under Contract No. DE-AC02-05CH11231. We acknowledge the Facility of Nanofabrication (FNF) of IOM for the support in sample preparation, Simone Dal Zilio and Silvio Greco for help in data analysis and stimulating discussions. We acknowledge Prof. Giuseppe Firrao for valuable comments and inspiring ideas, the NanoInnovation laboratory (Elettra Sincrotrone) for suggestion provided for AFM analysis and the BioLab (Elettra Sincrotrone) for the use of lab and instrumentation.

Electronic Supplementary Material: Supplementary material (further details of the SEM, TEM, cryo-EM, AFM SAXS characterization and analysis on fit procedure for LSPR measurements) is available in the online version of this article at https://doi.org/10.1007/s12274-019-2535-0.

References

[1] Ghosh, S. K.; Pal, T. Interparticle coupling effect on the surface plasmon resonance of gold nanoparticles: From theory to applications. *Chem. Rev.* **2007**, *107*, 4797–4862.

[2] Reinhard, B. M.; Siu, M.; Agarwal, H.; Alivisatos, A. P.; Liphardt, J. Calibration of dynamic molecular rulers based on plasmon coupling between gold nanoparticles. *Nano Lett.* **2005**, *5*, 2246–2252.

[3] Prodan, E.; Radloff, C.; Halas, N. J.; Nordlander, P. A hybridization model for the plasmon response of complex nanostructures. *Science* **2003**, *302*, 419–422.

[4] Hill, R. T.; Mock, J. J.; Hucknall, A.; Wolter, S. D.; Jokerst, N. M.; Smith, D. R.; Chilkoti, A. Plasmon ruler with angstrom length resolution. *ACS Nano* **2012**, *6*, 9237–9246.

[5] Zhang, J.; Fu, Y.; Chowdhury, M. H.; Lakowicz, J. R. Metal-enhanced single-molecule fluorescence on silver particle monomer and dimer: Coupling effect between metal particles. *Nano Lett.* **2007**, *7*, 2101–2107.

[6] Lim, D. K.; Jeon, K. S.; Kim, H. M.; Nam, J. M.; Suh, Y. D. Nanogap-engineerable Raman-active nanodumbbells for single-molecule detection. *Nat. Mater.* **2010**, *9*, 60–67.

[7] Taminiau, T. H.; Stefani, F. D.; Segerink, F. B.; Van Hulst, N. F. Optical antennas direct single-molecule emission. *Nat. Photonics* **2008**, *2*, 234–237.

[8] Bek, A.; Jansen, R.; Ringler, M.; Mayilo, S.; Klar, T. A.; Feldmann, J. Fluorescence enhancement in hot spots of AFM-designed gold nanoparticle sandwiches. *Nano Lett.* **2008**, *8*, 485–490.

[9] Ding, B. Q.; Deng, Z. T.; Yan, H.; Cabrini, S.; Zuckermann, R. N.; Bokor, J. Gold nanoparticle self-similar chain structure organized by DNA origami. *J. Am. Chem. Soc.* **2010**, *132*, 3248–3249.

[10] Zhou, C.; Duan, X. Y.; Liu, N. A plasmonic nanorod that walks on DNA origami. *Nat. Commun.* **2015**, *6*, 8102.

[11] Kuzyk, A.; Schreiber, R.; Fan, Z. Y.; Pardatscher, G.; Roller, E. M.; Högele, A.; Simmel, F. C.; Govorov, A. O.; Liedl, T. DNA-based self-assembly of chiral plasmonic nanostructures with tailored optical response. *Nature* **2012**, *483*, 311–314.

[12] Rothemund, P. W. K. Folding DNA to create nanoscale shapes and patterns. *Nature* **2006**, *440*, 297–302.

[13] Zanacchi, F. C.; Manzo, C.; Alvarez, A. S.; Derr, N. D.; Garcia-Parajo, M. F.; Lakadamyali, M. A DNA origami platform for quantifying protein copy number in super-resolution. *Nat. Methods* **2017**, *14*, 789–792.

[14] Hudoba, M. W.; Luo, Y.; Zacharias, A.; Poirier, M. G.; Castro, C. E. Dynamic DNA origami device for measuring compressive depletion forces. *ACS Nano* **2017**, *11*, 6566–6573.

[15] Hong, F.; Zhang, F.; Liu, Y.; Yan, H. DNA origami: Scaffolds for creating higher order structures. *Chem. Rev.* **2017**, *117*, 12584–12640.

[16] Jiang, Q.; Song, C.; Nangreave, J.; Liu, X. W.; Lin, L.; Qiu, D. L.; Wang, Z. G.; Zou, G. Z.; Liang, X. J.; Yan, H. et al. DNA origami as a carrier for circumvention of drug resistance. *J. Am. Chem. Soc.* **2012**, *134*, 13396–13403.

[17] Hemmig, E. A.; Fitzgerald, C.; Maffeo, C.; Hecker, L.; Ochmann, S. E.; Aksimentiev, A.; Tinnefeld, P.; Keyser, U. F. Optical voltage sensing using DNA origami. *Nano Lett.* **2018**, *18*, 1962–1971.

[18] Marini, M.; Piantanida, L.; Musetti, R.; Bek, A.; Dong, M. D.; Besenbacher, F.; Lazzarino, M.; Firrao, G. A revertible, autonomous, self-assembled DNA-origami nanoactuator. *Nano Lett.* **2011**, *11*, 5449–5454.

[19] Torelli, E.; Marini, M.; Palmano, S.; Piantanida, L.; Polano, C.; Scarpellini, A.; Lazzarino, M.; Firrao, G. A DNA origami nanorobot controlled by nucleic acid hybridization. *Small* **2014**, *10*, 2918–2926.

[20] Prinz, J.; Schreiber, B.; Olejko, L.; Oertel, J.; Rackwitz, J.; Keller, A.; Bald, I. DNA origami substrates for highly sensitive surface-enhanced Raman scattering. *J. Phys. Chem. Lett.* **2013**, *4*, 4140–4145.

[21] Acuna, G. P.; Möller, F. M.; Holzmeister, P.; Beater, S.; Lalkens, B.; Tinnefeld, P. Fluorescence enhancement at docking sites of DNA-directed self-assembled nanoantennas. *Science* **2012**, *338*, 506–510.

[22] Piantanida, L.; Naumenko, D.; Lazzarino, M. Highly efficient gold nanoparticle dimer formation via DNA hybridization. *RSC Adv.* **2014**, *4*, 15281–15287.

[23] Sönnichsen, C.; Reinhard, B. M.; Liphardt, J.; Alivisatos, A. P. A molecular ruler based on plasmon coupling of single gold and silver nanoparticles. *Nat. Biotechnol.* **2005**, *23*, 741–745.

[24] Kuzyk, A.; Urban, M. J.; Idili, A.; Ricci, F.; Liu, N. Selective control of reconfigurable chiral plasmonic metamolecules. *Sci. Adv.* **2017**, *3*, e1602803.

[25] Zhou, C.; Xin, L.; Duan, X. Y.; Urban, M. J.; Liu, N. Dynamic plasmonic system that responds to thermal and aptamer-target regulations. *Nano Lett.* **2018**, *18*, 7395–7399.

[26] Schreiber, R.; Luong, N.; Fan, Z. Y.; Kuzyk, A.; Nickels, P. C.; Zhang, T.; Smith, D. M.; Yurke, B.; Kuang, W.; Govorov, A. O. et al. Chiral plasmonic DNA nanostructures with switchable circular dichroism. *Nat. Commun.* **2013**, *4*, 2948.

[27] Piantanida, L.; Naumenko, D.; Torelli, E.; Marini, M.; Bauer, D. M.; Fruk, L.; Firrao, G.; Lazzarino, M. Plasmon resonance tuning using DNA origami actuation. *Chem. Commun.* **2015**, *51*, 4789–4792.

[28] Kim, D. N.; Kilchherr, F.; Dietz, H.; Bathe, M. Quantitative prediction of 3D solution shape and flexibility of nucleic acid nanostructures. *Nucleic Acids Res.* **2012**, *40*, 2862–2868.

[29] Castro, C. E.; Kilchherr, F.; Kim, D. N.; Shiao, E. L.; Wauer, T.; Wortmann, P.; Bathe, M.; Dietz, H. A primer to scaffolded DNA origami. *Nat. Methods* **2011**, *8*, 221–229.

[30] Masciotti, V.; Naumenko, D.; Lazzarino, M.; Piantanida, L. Tuning gold nanoparticles plasmonic properties by DNA nanotechnology. In *DNA Nanotechnology: Methods and Protocols*. Zuccheri, G., Ed.; Springer: New York, NY, 2018; pp 279–297.

[31] Dubochet, J.; Adrian, M.; Chang, J. J.; Homo, J. C.; Lepault, J.; McDowall, A. W.; Schultz, P. Cryo-electron microscopy of vitrified specimens. *Quart. Rev. Biophys.* **1988**, *21*, 129–228.

[32] Glaeser, R. M. Retrospective: Radiation damage and its associated "information limitations". *J. Struct. Biol.* **2008**, *163*, 271–276.

[33] Lei, D. S.; Marras, A. E.; Liu, J. F.; Huang, C. M.; Zhou, L. F.; Castro, C. E.; Su, H. J.; Ren, G. Three-dimensional structural dynamics of DNA origami Bennett linkages using individual-particle electron tomography. *Nat. Commun.* **2018**, *9*, 592.

[34] Zhang, L.; Lei, D. S.; Smith, J. M.; Zhang, M.; Tong, H. M.; Zhang, X.; Lu, Z. Y.; Liu, J. K.; Alivisatos, A. P.; Ren, G. Three-dimensional structural

dynamics and fluctuations of DNA-nanogold conjugates by individual-particle electron tomography. *Nat*. *Commun*. **2016**, *7*, 11083.

[35] Amenitsch, H.; Rappolt, M.; Kriechbaum, M.; Mio, H.; Laggner, P.; Bernstorff, S. First performance assessment of the small-angle X-ray scattering beamline at ELETTRA. *J*. *Synchrotron Radiat*. **1998**, *5*, 506–508.

[36] Bernstorff, S.; Amenitsch, H.; Laggner, P. High-throughput asymmetric double-crystal monochromator of the SAXS beamline at ELETTRA. *J*. *Synchrotron Radiat*. **1998**, *5*, 1215–1221.

[37] Forget, A.; Pique, R. A.; Ahmadi, V.; Lüdeke, S.; Shastri, V. P. Mechanically tailored agarose hydrogels through molecular alloying with β-sheet polysaccharides. *Macromol*. *Rapid Commun*. **2015**, *36*, 196–203.

[38] Rüther, A.; Forget, A.; Roy, A.; Carballo, C.; Mießmer, F.; Dukor, R. K.; Nafie, L. A.; Johannessen, C.; Shastri, V. P.; Lüdeke, S. Unravelling a direct role for polysaccharide β-strands in the higher order structure of physical hydrogels. *Angew*. *Chem*., *Int*. *Ed*. **2017**, *56*, 4603–4607.

[39] Mie, G. Beiträge zur Optik trüber Medien, speziell kolloidaler Metallösungen. *Ann*. *Phys*. **1908**, *330*, 377–445.

[40] García De Abajo, F. J. Multiple scattering of radiation in clusters of dielectrics. *Phys*. *Rev*. *B* **1999**, *60*, 6086–6102.

[41] Myroshnychenko, V.; Rodríguez-Fernández, J.; Pastoriza-Santos, I.; Funston, A. M.; Novo, C.; Mulvaney, P.; Liz-Marzán, L. M.; García De Abajo, F. J. Modelling the optical response of gold nanoparticles. *Chem*. *Soc*. *Rev*. **2008**, *37*, 1792–1805.

[42] Walsh, A. S.; Yin, H. F.; Erben, C. M.; Wood, M. J. A.; Turberfield, A. J. DNA cage delivery to mammalian cells. *ACS Nano* **2011**, *5*, 5427–5432.

[43] Lee, H.; Lytton-Jean, A. K. R.; Chen, Y.; Love, K. T.; Park, A. I.; Karagiannis, E. D.; Sehgal, A.; Querbes, W.; Zurenko, C. S.; Jayaraman, M. et al. Molecularly self-assembled nucleic acid nanoparticles for targeted *in vivo* siRNA delivery. *Nat*. *Nanotechnol*. **2012**, *7*, 389–393.

Electronic Supplementary Material

A DNA origami plasmonic sensor with environment-independent read-out

Valentina Masciotti[1,2] (✉), Luca Piantanida[1,†], Denys Naumenko[1,3], Heinz Amenitsch[4], Mattia Fanetti[5], Matjaž Valant[5,6], Dongsheng Lei[7,8], Gang Ren[7], and Marco Lazzarino[1] (✉)

[1] *CNR-IOM, AREA Science Park, Basovizza Trieste I-34149, Italy*
[2] *PhD Course in Nanotechnology, University of Trieste, Trieste I-34127, Italy*
[3] *Institute for Physics of Semiconductors, National Academy of Sciences of Ukraine, Kyiv 03028, Ukraine*
[4] *Institute of Inorganic Chemistry, Graz University of Technology, Graz A-8010, Austria*
[5] *Materials Research Laboratory, University of Nova Gorica, Nova Gorica SI-5000, Slovenia*
[6] *Institute of Fundamental and Frontier Sciences, University of Electronic Science and Technology of China, Chengdu 610054, China*
[7] *The Molecular Foundry, Lawrence Berkeley National Laboratory, Berkeley CA 94720, USA*
[8] *School of Physical Science and Technology, Electron Microscopy Center of LZU, Lanzhou University, Lanzhou 730000, China*
[†] *Present address: Micron School of Materials Science & Engineering, Boise State University, Boise, ID 83725, USA*

Supporting information to https://doi.org/10.1007/s12274-019-2535-0

Index

1. The design

Each edge of the wireframe DNA origami tetrahedron is composed of four dsDNA helix ~90 nm long and is connected to the other two neighboring edges at the vertices by flexible joints. The scaffold strand, coming out from the struts, crosses each vertices twice. The connection points between the struts are composed by 5 bases left at single strand. The number of bases composing three of the six struts slightly differ to fold completely the scaffold strand. Three of the struts have been designed with a central seam which separates the two half of the pillar itself, so we properly prolonged the staples strands tuning their pairing to build a cage around the seam in order to reinforce the central part. In the three pillars left, the scaffold strand still forms a central seam but the external helix extends along the entire length of the pillar maintaining the struts more robust (Fig. S1).

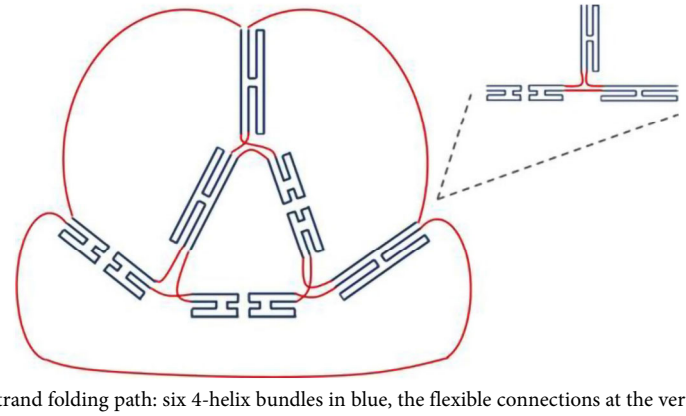

Figure S1 Visual model of the scaffold strand folding path: six 4-helix bundles in blue, the flexible connections at the vertices in red. There are two different types of struts: the two half struts typology and the strut with a central seam. On the right side, a focus of the vertex connection.

Address correspondence to Valentina Masciotti, masciotti@iom.cnr.it; Marco Lazzarino, lazzarino@iom.cnr.it

Two different sets of staples fold the two struts involved in the probe-target actuation facet: (i) staples pair the entire scaffold strand of the struts (0ss), (ii) staples leave unpaired 4 nucleotides of three helices of the struts (3ss) (Fig. S2). The purpose was to plan two different tetrahedral DNA origami characterized by different mechanical properties.

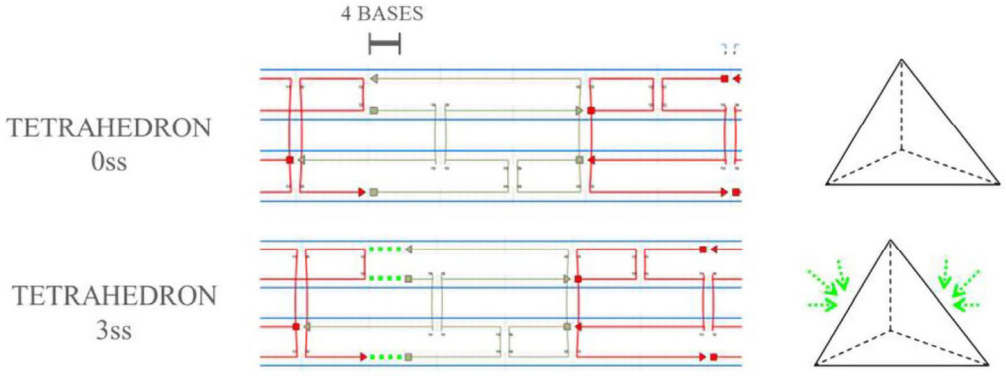

Figure S2 Two set of staples containing: no single strand (0ss) and 4-single strands bases in 3 helices (3ss). The scaffold strand is blue, the structural staples strands are red, the staples involved in the variable part of the struts are grey, and the green dotted segments are the 4-bases gaps where the scaffold strand is left unpaired. On the right, the arrows indicate the position and the number of weak points.

0ss and 3ss have been separately designed through the help of design-assisted software caDNAno; the list of nucleotide sequences of staple strands, catchers strands, probe and target are shown in section 7.

2. Purification and additional characterization

The purification of the folded structure from excess of staples strands has been initially operated through Amicon filtration. In Figure S3(a) is shown an UV image of agarose gel: in the first and in the third lanes we can observe the migration of the ladder and of the M13mp18 while the forth and the fifth wells were filled with DNA origami tetrahedron respectively before and after the Amicon purification. The red box in Figure S3(a) identifies the gel bands corresponding to the well folded origami. As expected, after the purification step the staples were removed and the origami concentration was increased (band brightness enhancement). Meanwhile we witnessed to the formation of two slower bands which correspond to larger constructs, probably derived from the aggregation of two and three tetrahedrons. SEM characterization confirmed the agarose gel indications: most of the tetrahedrons analyzed were aggregated (Fig. S3(b),(c)) or broken in different places, probably because of the harsh purification step. These results suggested that the purification of the DNA origami tetrahedron with Amicon was not successful; for this reason no staple purification has been used in all the performed experiments.

The DNA origami concentration was calculated using ImageJ software: the brightness of the whole lane can be assumed proportional to the M13mp18 initial concentration (10 nM), so the ratio between the brightness of the origami band and of the entire lane is equivalent to the ratio between the concentration of the scaffold strand and of the origami tetrahedron. SEM analysis did not highlight structural differences among 0ss and 3ss tetrahedrons.

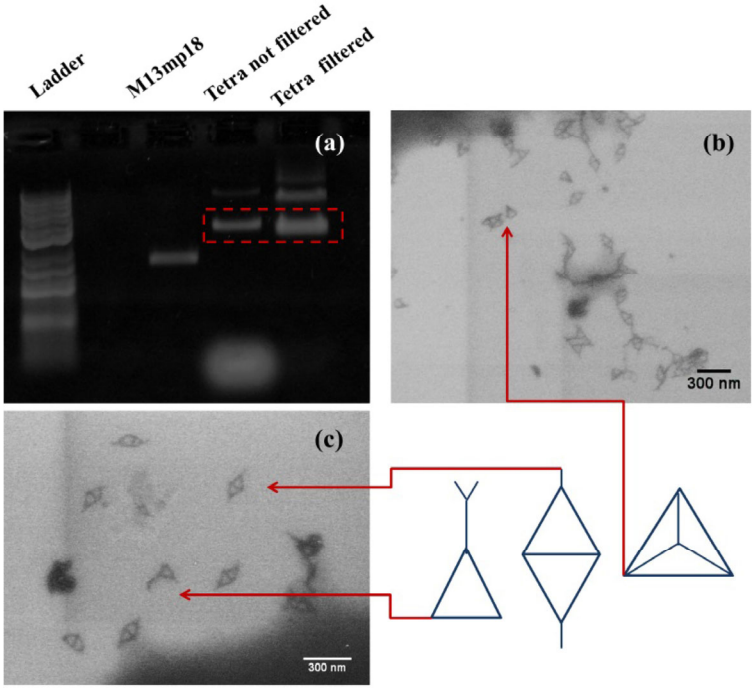

Figure S3 (a) Agarose gel electrophoresis of DNA origami tetrahedron shows the concentration and the aggregation enhancement after Amicon purification, M13mp18 is used as a control of the folding success; (b) and (c) SEM pictures in which there are well-folded tetrahedron, broken and aggregated DNA architectures.

The anchoring of AuNP to the DNA origami was extrapolated from agarose gel analysis: first we calculated the DNA origami concentration from the fluorescence intensity of well folded DNA origami band compared to the intensity of the entire lane as described above. Since the total amount of M13 in the sample was 6.25 nM and we loaded 10 μl in each well of the gel we can estimate the concentration of well folded DNA origami present in the bands of interest. In the same way we calculated the AuNP absorbance and we obtained the ratio between the absorbance in the band of interest and the entire lane. Since the initial concentration of AuNP was 6.25 nM, the ratio AuNP: M13 is 1:1 while the ratio AuNP: well folded DNA origami tetrahedron is 4:1. Since the band of interest may contain tetrahedron without AuNP, tetrahedrons with only one AuNP, and tetrahedron correctly formed with 2 AuNP, we further needed to evaluate the relative probability of these three configurations. We analyzed 220 DNA origami from 50 SEM pictures and we found out 115 structures with AuNP dimers, 105 structures with a single AuNP: therefore, we assumed a ratio between dimer and single NP of 1:1.

Finally, from the gel presented in Figure 1 the yield of dimers obtained was (1) 13% for 0ss, (2) 8.3% for 0ss+Target, (3) 10% for 3ss and (4) 10% for 3ss+Target.

3. AFM analysis of the kite-like DNA origami

AFM analysis was performed in contact mode in air [S1, S2], on the "kite-like" DNA origami and we observed that that almost all the structures were in the flat configuration, except few of them which were folded on themselves (Fig. S4(a)), probably because the scaffold strand can still pull the two halves of the broken strut together. Moreover, the flexibility of the vertices provides enough degrees of freedom to allow the folding of the structure on itself even if it is statistically less probable, due to the electrostatic repulsion between the origami struts. The profile of the kite-like DNA origami deposited on mica as measured from the topographic images, post-processed with Gwyddion software, highlights an average strut height of 2 nm which is substantially lower than 2 double-helix value in solution (between 4 and 5 nm) (Fig. S4(b),(d))[S3]. Numerically the same results were obtained also in tapping mode in liquid but with a lower image quality. These discrepancies are often observed when imaging in air with AFM because of a combination effects of water drying and AFM tip pressure, therefore these measurements are usually considered only indicative [S4]. The apparent width of the dsDNA molecules is strictly correlated with the tip used, but it was always exceeding the 2 dsDNA diameter in solution, which is to be expected for tips with apex radii exceeding substantially the molecular diameter (Fig. S4(c)).

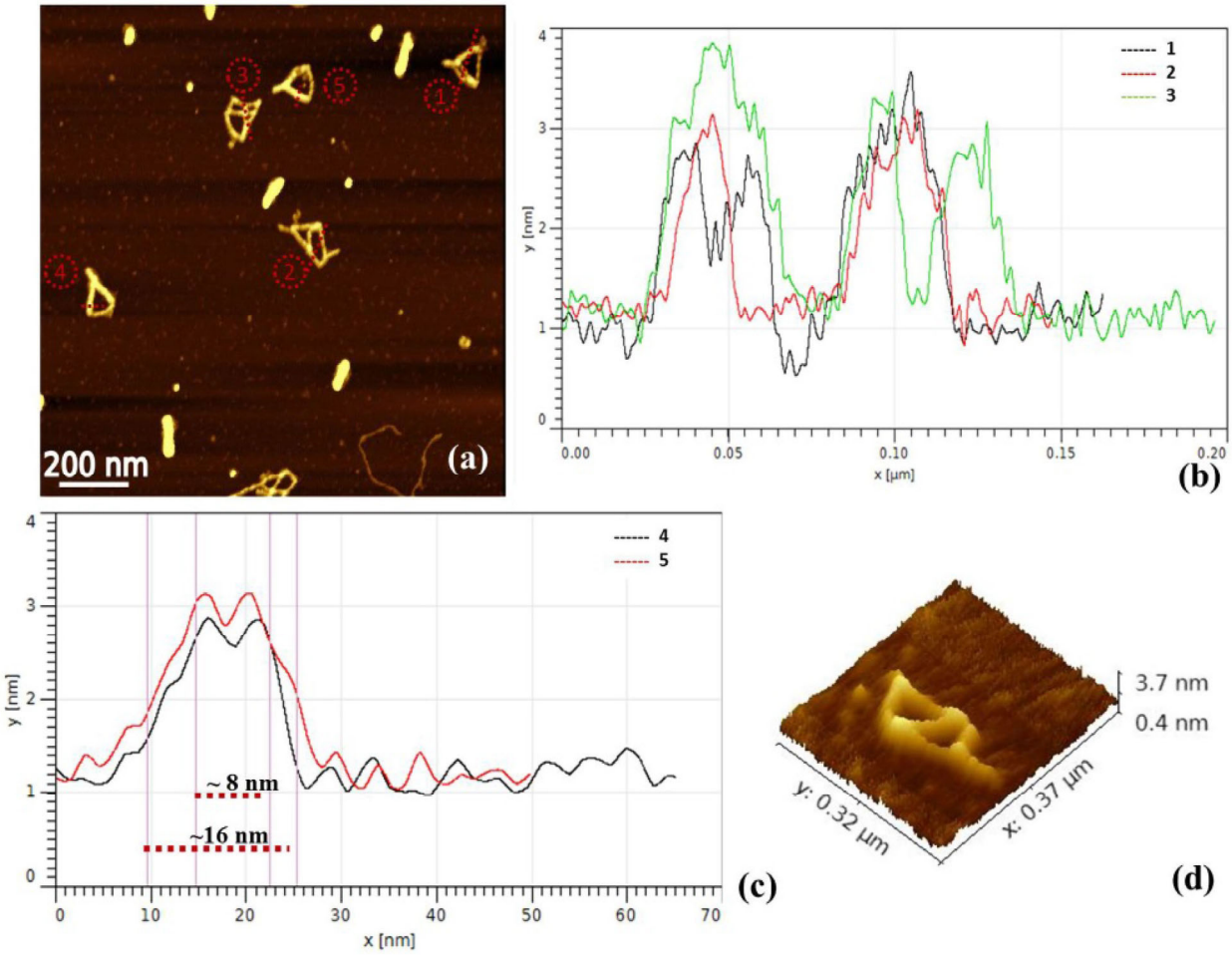

Figure S4 (a) AFM image of the flat version of tetrahedral DNA origami, few of them are folded on themselves; (b) height profile of the structures shown in Figure 3.1(a); (c) width of the kite-like struts using Gwyddion tool; (d) 3D AFM image of a kite-like DNA origami.

4. Additional SEM and TEM and Cryo-EM characterization

Transmission electron (TEM) and cryo-electron microscope (cryo-EM) have been used in combination with scanning electron microscope (Fig. 1(d)) to validate the folding of the tetrahedron (Fig. S7).

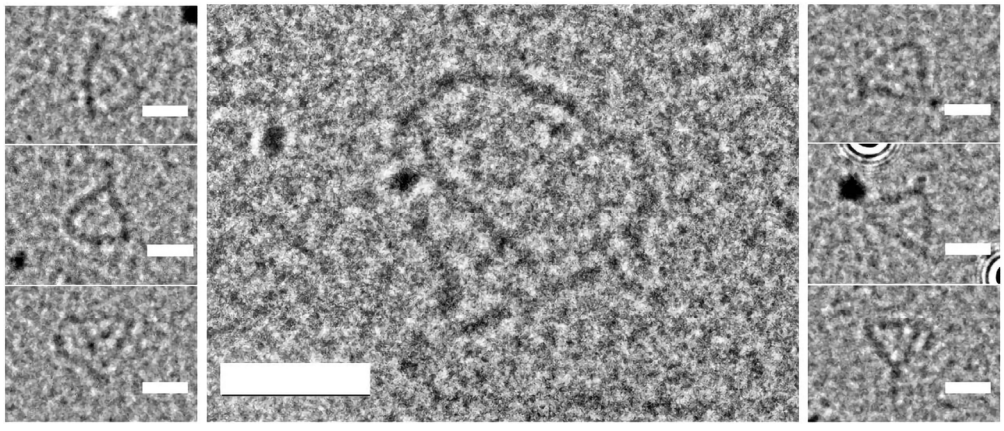

Figure S5 TEM images representing the well-folded tetrahedron shown in Figure 1(d) (scale bar 50 nm).

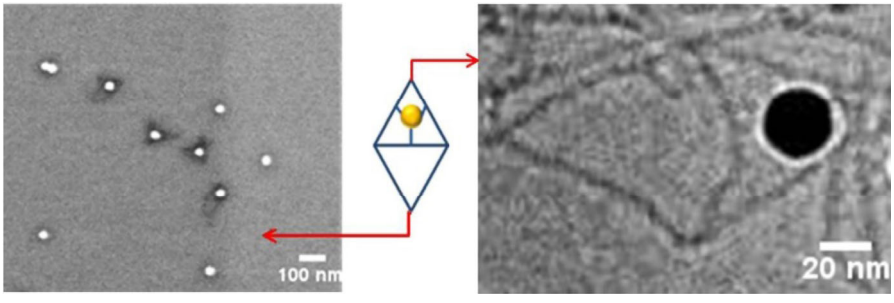

Figure S6 DNA origami tetrahedron conjugated with one AuNP: on the left SEM image with a broken tetrahedron in which is visible the right AuNP positioning; on the right cryo-EM of a broken tetra with one AuNP confirmed the central positioning of the AuNP in one *AuNP facet*.

In order to selectively decorate the DNA origami structure with one or two gold nanoparticles, we initially synthesized it using only one set of catchers strand which are involved in the binding of one AuNP.

The conjugation of one AuNP to the DNA tetrahedron, still allows to visualize the tetrahedral shape. Moreover, the presence of kite-like structure, as in Figure S6, evidences the precise positioning of the AuNP in the center of a tetrahedral facet.

Further functionalization with the second gold nanoparticles has been performed through the addition in the DNA origami synthesis mix of another set of catcher strands, recognizing the same AuNP functionalization. The presence of a second NP attached to the tetrahedral architecture, further increases the signal background, coming from secondary electrons scattered by the two nanoparticles, thus outshining the signal generated by the origami itself. In some cases, the triangular shadow, attributable to DNA origami, can be still observed (Fig. S7).

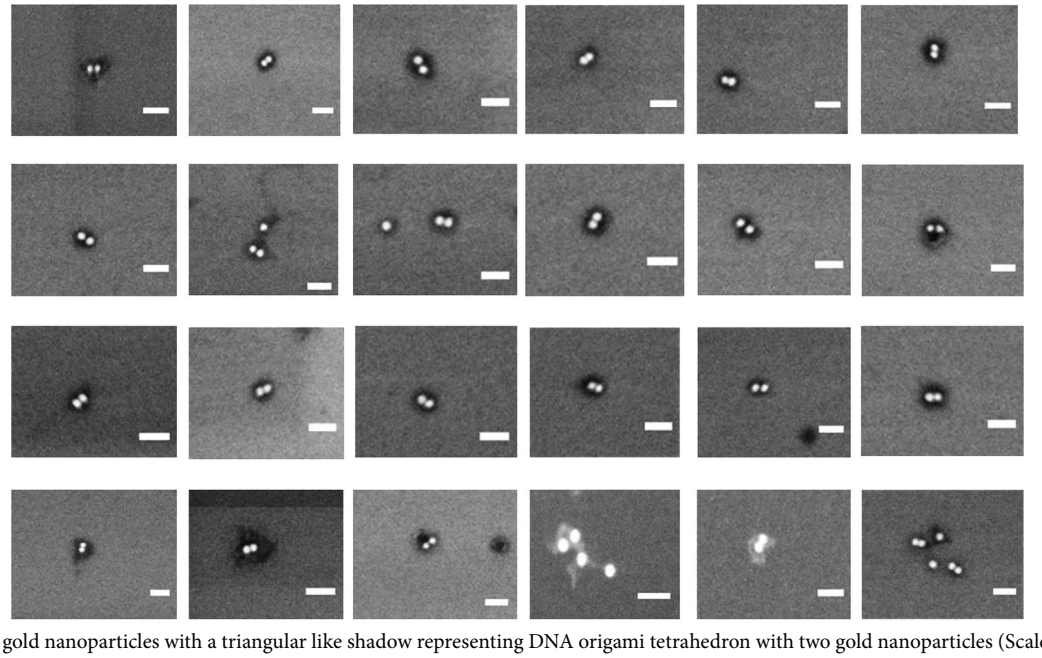

Figure S7 Dimers of gold nanoparticles with a triangular like shadow representing DNA origami tetrahedron with two gold nanoparticles (Scale bar 100 nm).

Cryo-EM characterization (Fig. S8) showed triangular like structures heterogeneously distributed in the grid, often anchored to the lacey carbon film formed net. Nonetheless, it is still possible to appreciate the presence of many AuNP dimers deriving from tetrahedrons not clearly distinguishable.

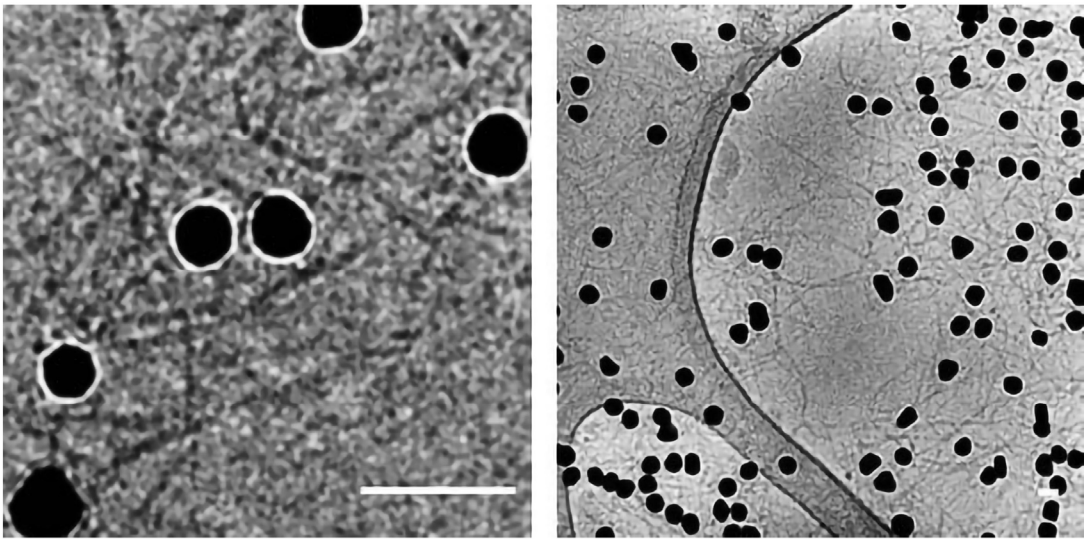

Figure S8 Cryo-EM images of dimers of gold nanoparticles with a triangular like DNA origami structures; in the second picture it is possible to appreciate that the hybrid AuNP-DNA origami structures are heterogeneously dispersed in close proximity of the lacey carbon film formed net (Scale bar 50 nm).

5. SAXS data

In order to facilitate the comparison between the SAXS pattern before and after the structure factor derivation in Figure S9 is shown the zoom of the data presented in Figure 2(a) and (b) restricted to the q-range of interest.

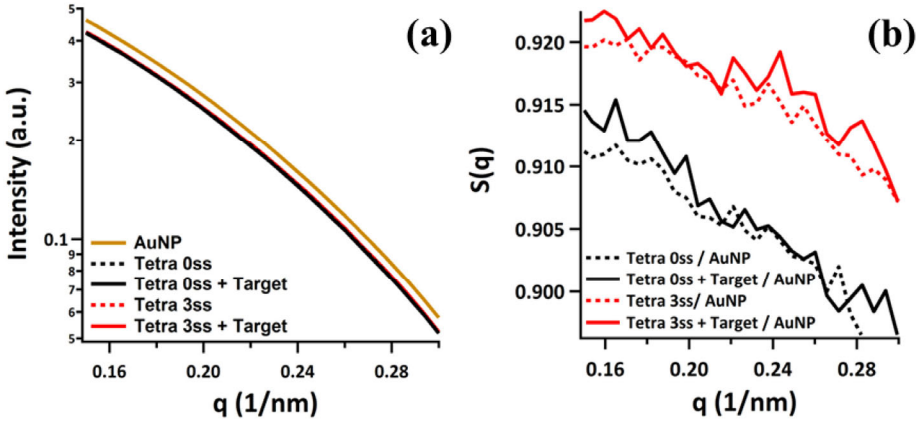

Figure S9 Zoom in the q-range of interest of SAXS data presented in Figure 2(a) and (b)in the main text. (a) Scattering pattern of all samples and the DNA-functionalized AuNP reference sample do not present significant peaks in the region of interest since the signal is mainly dominated by free AuNP in solution; (b) to extract the particle-particle interference, the structure factor has been derived by dividing the pattern with the AuNP signal (gold-yellow line). The structure factor of the different tetrahedrons highlights the presence of differences only between 3ss before and after target hybridization while no relevant variability has been recorded in 0ss structures after target addition.

6. LSPR analysis

A basic equation to calculate the actual extinction spectra is:

$$A + S + R + T = 1 \quad (1)$$

where A is absorption, S is scattering, R is reflection and T is transmission of the light and A+S= E represents the extinction. Neglecting the difference in the light reflection from the surface of clean gel and the one with AuNP, E = 1- T. Thus, the final equation to calculate the extinction is:

$$E = (I_0 - I_i)/(I_0 - I_{bg}) \quad (2)$$

where I_i is the corresponding intensity of light passed through each band, and I_0 is the intensity of light passed through the clean gel in a position without origami and nanoparticles. I_{bg} is a dark thermal noise of CCD. At least 5 different positions along each band have been characterized and finally averaged [S5].

6.1 LSPR measurements in liquid

The measurements in liquid have been performed in a home-made cell fabricated from a PMMA slab with two coverslip glasses attached to both sides. 10 μl of liquid sample was loaded in the chamber preliminary created in the slab avoiding the formation of air bubbles.

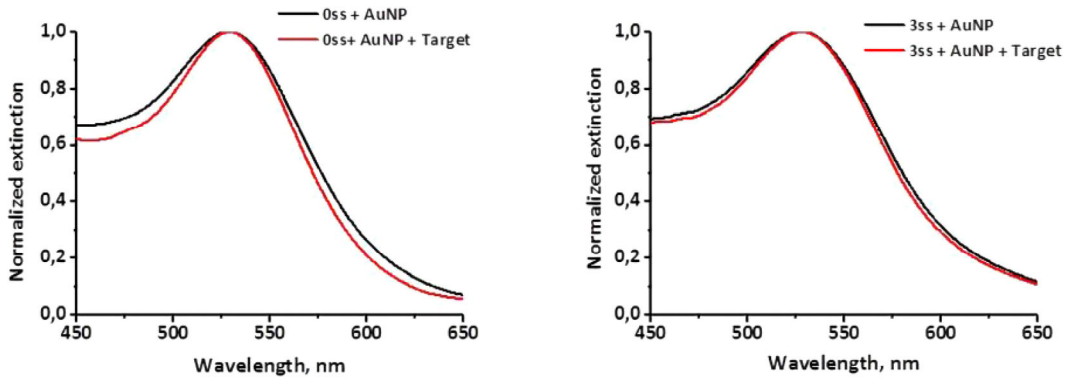

Figure S10 Extinction spectra of AuNP-tetrahedral DNA origami in solution before and after the probe-target actuation of 0ss and 3ss respectively demonstrating that LSPR shift cannot be observed. In both samples the target addition does not shift the plasmon resonance for the contribution of free AuNP dominating the spectra, as discussed in the main text. However, we observed that in both cases after the target addition the resonance width decreases, as a consequence of the greater stability conferred to the structure by the hybridized probe, and the subsequent reduction of thermal fluctuations.

6.2 LSPR measurements in gel and data treatment

The extinction spectra show a peak in the range of 525-535 nm which is attributed to the LSPR in single gold AuNP or dimers. The spectra in gel demonstrate a different extinction at short wavelengths complicating an estimation of LSPR position. Since the gel density, gel hydration and AuNP size in each series of experiments are supposed to be constant the difference in the extinction is caused by a variable gel thickness of the lanes.

The best agreement between the experimental data for single DNA-coated AuNP in liquid and simulations was obtained with $\varepsilon_{eff} = 2.0$ which in terms of effective medium approximation (EMA) corresponds to $\varepsilon_{eff} = 0.34 \cdot \varepsilon_{DNA} + 0.66 \cdot \varepsilon_{water}$, where $\varepsilon_{DNA} = 2.450$ and $\varepsilon_{water} = 1.769$ are dielectric permittivity of DNA and water respectively. The ε_{eff} in gel increases by 1% since dielectric permittivity of gel is higher than of water ($\varepsilon_{gel} = 1.796$). The experimental data displayed in Figure 3(c) were fitted with 2 Gaussian curves (Fig. S11), each of them represents the particular extinction process and is related to: i) plasmon excitation in AuNP dimer, ii) variation in gel thickness and/or structure. The first term was fully variable while the wavelength position and the peak width of the second were fixed and obtained from the measurements of clean gel (Fig. S12). Notice that the peak height was variable in the second case.

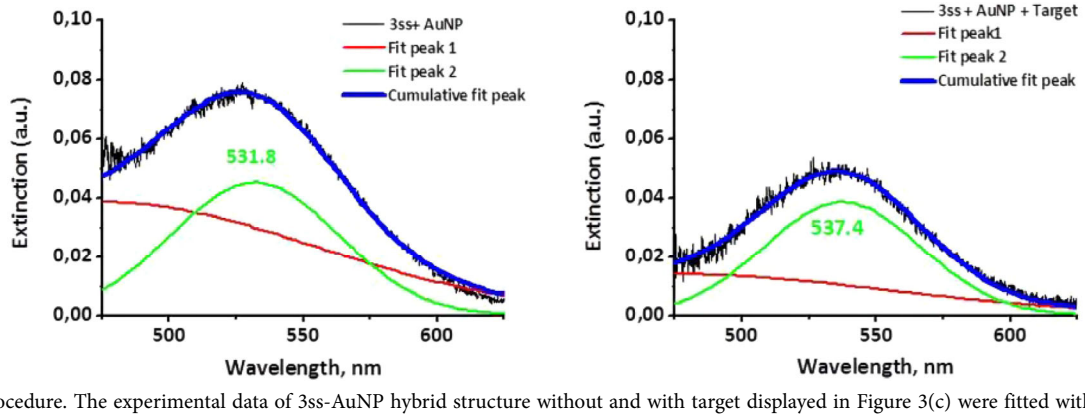

Figure S11 it procedure. The experimental data of 3ss-AuNP hybrid structure without and with target displayed in Figure 3(c) were fitted with 2 Gaussian curves, each of them represents the particular extinction process and is related to: plasmon excitation in AuNP dimer (green curve), variation in gel thickness (red curve).

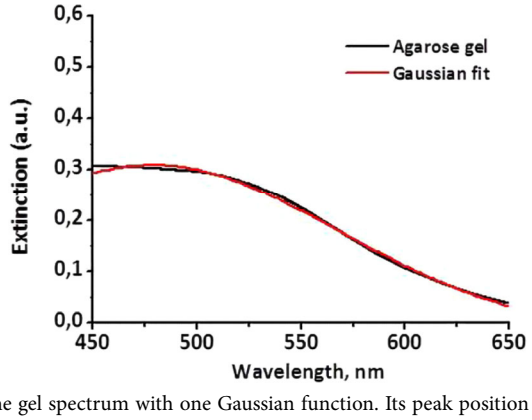

Figure S12 The image below represents a fit of the gel spectrum with one Gaussian function. Its peak position will be fixed at 475 nm, a width at 160 nm, while a height will be variable.

7. Table of nucleotide sequences

Table S1 List of the nucleotides sequences used for the synthesis of the DNA origami tetrahedron structures (ST). The catchers strand for the anchoring of AuNP positioned in the facet 1 and 2 are named 1NP and 2NP: the black sequence is complementary with the structure sequence, while the green sequences represents the region complementary to the AuNP sequence and the red part in the linker. The catchers for the actuator strand and the actuator strand. Two different sets of staples strand have been used for the synthesis of the DNA origami tetrahedron 0ss and 3ss.

NAME	Sequence 5' ----->3'	Length (nt)	
ST1	AAATCAAATTTAATTGACGGTGTCTGGAAGTT	32	
ST2	ATAGCCGAACAGAGATGGTTTA	22	
ST3	GTAAAGCACAAGTTTTCCAACGTCAAAGGGCG	32	
ST4	ACCACATTGATAGCGTCTAATGCAGAACGCGC	32	
ST5	TGCCTGCAACAACATAGGCGCCAGGGTGGTTT	32	
ST6	CGTATTAATTCCGAAAGACGGGGAAAGCCGGC	32	
ST7	ACCACCGGATCAAAATGAACAAGATGATATTC	32	
ST8	CTAAATCGTTTTGCGGCTCAGAGC	24	
ST9	AAGGGAACTAAAACGACTTATTACGCAGTATG	32	
ST10	TTCTTTTCTGGGTTATCTAGAGGATCCCCGGG	32	
ST11	AGTGTACTGGTAATAAGTT	19	
ST12	GAATTGAGAGCCGTTTACAGCCATATTATTTA	32	
ST13	AAATTCTTCAATAGGATTCCGGCA	24	
ST14	CTTGCTTCAATCAATAATTTCAATTACCTGAG	32	
ST15	CTCATTTTGTCAATAAAAACAAGA	24	
ST16	GGCAATTCTAAGACGCGTAGATTTTCAGGTTT	32	
ST17	ATAAGAATAAATGTGAGCATCTGCCAGTTTGA	32	
ST18	TATTACAGCTGAATATGTAATTCTGAATCCCC	32	
ST19	TAACTCACCGCCAGGGAAATATATTTTAGTTA	32	
ST20	ACAAACAAGTCAGACGCCCTCAGAGCCGCCAC	32	
ST21	GTAAATATAAATGAATCGCCCACGCATAACCGATA	35	
ST22	CACTAACAACAGTTGACAGCAAGCGGTCCACG	32	
ST23	TCAACATTAAACACCGTGTTGGGAAGGGCGAT	32	
ST24	TCACCCTCGCTTGATAACAGTTTCAGCGGAGT	32	
ST25	ATTTCATCAGTCGGGACGTTGCGCTCACTGCC	32	
ST26	GCTGATGCGCGTATTGCGAGCCGGAAGCATAA	32	
ST27	ATTTGGGAATACATGGCAAGTTTGCCTTTAGC	32	
ST28	TTTAAAAGCCCCAGCAGAAGGGAAGTCAGTTG	32	
ST29	CTTTACAATAGAGCTTTCGGCAAAATCCCTTA	32	
ST30	TAAAACGAATGTTCAGCCAATACT	24	
ST31	AACAATGAAAACCAAGAAACGATTTTTTGTTT	32	
ST32	TTAGACTGCAACTAATGAAAAATCTACGTTAA	32	
ST33	GCCAGTAAACTAAAGTCTCCTTTTGATAAGAG	32	
ST34	TAATTAATTTTCCCTTTGAATTACAACAAACATCAAGAAA	40	
ST35	AGTACATATGTAAATCAATAACGGATTCGCCT	32	
ST36	TAAATCAATCTATCAGCACTACGTGAACCATC	32	
ST37	GGGGACGATGCGCAACGAATCATAATTACTAG	32	
ST38	CAATTCTATAAATTGTTAATCAGAAAAGCCCC	32	
ST39	GCCAGTTAGAGCAAGATAAATATAACCCACAA	32	
ST40	TTTTCATAAACCGCCTATTGGCCTGTCCACTA	32	
ST41	GGAATAAGTTTTTTCAGGAGCCTTTAATTGTA	32	
ST42	GAATTAGCAAAATTAAGATAAAAAGCCGGAGAACCGCCAC	40	
ST43	GCTTAGATATCAATATGTTTGGATTATACTTC	32	

ST44	AGAGTACCAATCAGGTGCAGAGGCATTTTCGA	32	
ST45	GCAGGGAGACAACCATTTTCTGTATGGGATTT	32	
ST46	AATTCATAAAAGGAACCTTTCGAGGTGAATTT	32	
ST47	ACCCAAATCTAAATCGCCCGAGAT	24	
ST48	CACCAACCCGAACTGATTACCCAAATCAACGT	32	
ST49	CGACGATAAAAACCAAACCCTCGTTCATTGTGAATTACCT	40	
ST50	AATCATTATGAAGCCTTTAGTTGCTATTTTGC	32	
ST51	CCTCAGAATACCGCCAGCCTCAGAGCATAAAG	32	
ST52	AAGAACCGCGTAGAAAAATGCCACTACGAAGG	32	
ST53	CACCAGAGCAGTCTCTTTTTCATCGGCATTTT	32	
ST54	GCCCGTATATAGTTAGTGCTCAGTACCAGGCG	32	
ST55	CTGCCTATCCATGTACACAACGCCAGGGTTGATATAAGTA	40	
ST56	CATTTCGCTATAAAGCGAAAGACT	24	
ST57	GCGCATAGAAAAAAGGTTTTTCATAACGCAAAGACACCAC	40	
ST58	CAAAAGAAGGAGAAACGTCGCTAT	24	
ST59	CACTAAAAAACGAGGCCAGTGAATAAGGCTTG	32	
ST60	CCAACATGTATAACAGAACAGGTCAGGATTAG	32	
ST61	TTTGTCGTGGGGTCAGCCTCAAGA	24	
ST62	TAGTCAGCAAACTCCTTGATTCCCAATTCTG	31	
ST63	TCCCAATCAAGTCAGAAATAATAAGAGCAAGA	32	
ST64	CAGCCCTCAAACAGTTCTGAAACATGAAAGTA	32	
ST65	GATTGCTTAATTATTCTATGTGAGCTAAGAAC	32	
ST66	ATTCAGGCCGACAGTACTGTAGCCAGCTTTCA	32	
ST67	GCTTAGGTACCAGTGAATTGTTATCCGCTCAC	32	
ST68	GCGAAAGGGGATAGGTACAAACGGCGGATTGA	32	
ST69	CAATAATCGGCTAAGAAAAGTA	22	
ST70	CCTGAACACAAATAAGTACCGCACTCATCGAG	32	
ST71	GTCAGACTGCCAAATCCAGCAACCAGAACCAC	32	
ST72	GAAAAATATTTAAGAACATAGTAAGAGCAACA	32	
ST73	AATAATAATTTATTTTACAGAGGCTTTGAGGA	32	
ST74	ATTTCATTAGAATCCTACAGTAACAGTACCTT	32	
ST75	TGAGGCAGATAAATCCATTAGCGTTTGCCATC	32	
ST76	TTCATTTGCGCATTAAACTAGCATGTCAATCA	32	
ST77	GACGACAATAAACAACACTAACGGGTTGAGATTTAGGAAT	40	
ST78	ATATCAGACAAAATAATTATTTTCATCGTAGG	32	
ST79	CAGACGTTAGTTGACGGAAATT	22	
ST80	AATTCCACGGTCGACTATAACTATATGTAAAT	32	
ST81	GGAGGTTTCCGCGCCCTTCCAGAGCCTAATTT	32	
ST82	AACGTCAGAATTGATTAATCCTACATTTAACA	32	
ST83	GCAAGGCAATAAACCCTCAGACAGTCAAA	29	
ST84	TGATAAATGAAAGTAAGCCTGGATTGTATAAG	32	
ST85	TCTAAAATATCTTTAGGAG	19	
ST86	AAAAACAGTAATGCCGAGTAGCATTAACATCC	32	
ST87	CAGAGGCGTGAATACCCCGGTATTTGAATAAC	32	
ST88	GAAATAAAGGAAGGGTCTGATTATCAGATGAT	32	
ST89	TTACATCGGATGATGACTTTTTTAATGGAAAC	32	
ST90	GATGGTGGATCCTTTGATTTAGAAGTATTAGA	32	
ST91	GTATCATCGCCTGATAAAT	19	

ST92	CCCTGACGAATAACGGTTTGACCCCCAGCGAT	32	
ST93	CCTGAGAGATCGTAAAATTTTTGTTAAATCAG	32	
ST94	GGCGGTTTAAATCCAACAGTGCCAAGCTTGCA	32	
ST95	AGGGCGACAACTTTCACCGATAGTTGCGCCGA	32	
ST96	GCCCTTTTTGTCTTTCATAGCAGCCTTTACAGAGA	35	
ST97	ATGTTTTAAATATGCATAAGAGAAAAACGAGAATGACCAT	40	
ST98	GATAATACCGAGAAAGGGCGAAAATCCTGTTT	32	
ST99	AAGGTAAAAATGCTGTGCTTAGAG	24	
ST100	ATCTCCAAGCTGGCTGATAAAAGAGAGGAAGTTTCCATTA	40	
ST101	TAAGCGTCATTAGAGCACCAGTAGCACCATTA	32	
ST102	GAAGGATTAGGATTAGCTGAGACTTGCCTTGAGTAACAGT	40	
ST103	GGCATGATTGCTCATTGCAGACGGTCAATCAT	32	
ST104	CTGGTTTGTTTGAGTAATTAGAGCCGTCAATA	32	
ST105	AACAAGCATTAAGCCCGGGTAATTGAGCGCTA	32	
ST106	AGGGTTGAGTGTTGTTCGTGGACTTTGGGGTCCCAGAGCC	40	
ST107	TTAAAATTGGGCGCGAGGCTATCAGGTCATTG	32	
ST108	TGAATAATGAAATTGCTGAGAAGAGTCAATAG	32	
ST109	AATAAATCAATGCAATTGTGTAGGTAAAGATT	32	
ST110	TTAAGAGGCGGGGTTTCGTAACGATCTAAAGT	32	
ST111	TGTAGAAAAACTTTAATTACCAGA	24	
ST112	TCAAATATCGCGTTTTGGAAGCCCCAACGCTCAACAGTAG	40	
ST113	CGGTCATACCGCCACCAGCATTGACAGGAGGT	32	
ST114	ACGCTAACACAATTTTAACCTCCCGACTTGCG	32	
ST115	AACGGGTAACGGTGTACAAGAGTAATCTTGAC	32	
ST116	GTGCCAGCTGCATTAAACTTTTTCTTTTCCCA	32	
ST117	GAATCGATGAACGGTATCTGGAGCCCTGTTTAGCTATATT	40	
ST118	CTTAATTGGTAGAAAGTATTCATTGTCCAGAC	32	
ST119	CGGGTATTAATAGCAAAGAATTAACTGAACAC	32	
ST120	CGGAATTATCATCAAAATCATA	22	
ST121	ATTATTTGCACGTAAAACA	19	
ST122	ATCGATAGCAGCACCGTAA	19	
ST123	TTGAGAGACCGGTTGAAAACGTTAATATTTTG	32	
ST124	CAATGACATTAAAGGCGATTGAGGGAGGGAAG	32	
ST125	ATATTTTAATACAGGCATTCAACCGTTCTAGC	32	
ST126	AACGTCAATAGACGGGTAGCTATCTTACCGAA	32	
ST127	GTCAGGACCAACAATAGGTAATAGTAAAATGT	32	
ST128	CTAAAGACCTCCAAAACGTTGAAA	24	
ST129	AACGCAATAGAAACACACCTGCTCCATGTTAC	32	
ST130	TGAATTTATCATATTCTAGAACCTACCATATCAAA	35	
ST131	CAAATATTCTAATAGTGAGAGGGTAGCTATTT	32	
ST132	GAGGGTAGTCAGCTTGAACTAAAGGAATTGCG	32	
ST133	CGCTTTCCTTCTGACCCTGCAAGGCGATTAAG	32	
ST134	AAATACCGCCGTGGGACACGTTGGTGTAGATG	32	
ST135	GGCAACATACCTTCATCAGACCAG	24	
ST136	TCAGTAGCAAGGCCGGGTCACCGACTTGAGCC	32	
ST137	CGGTGCGGGTAACCGTGCGAGTAACAACCCGT	32	
ST138	CGAACGAGTGAGAATCCGGATTGCATCAAAAA	32	
ST139	TGTGTCGAGCGCGAAAAGAAGGAAACCGAGGA	32	
ST140	CCCCGATTACATGGCCGGCGAATTCGACAACT	32	

ST141	TATACCAAAATCCGCGCAGAACGAGTAGTAAA	32	
ST142	CTTAAACAAGCAGCGACAGCGCCAAAGACAAA	32	
ST143	GATAAGTGCTATTATTAATGCCCC	24	
ST144	TTAAAGAACCAGTTTGCACCGGAAGAGGTGCC	32	
ST145	GGAAAGCGCCGCCGCCCTCAGAGCCACCACCC	32	
ST146	CCTCAGAAGCCCCCTTTCATTAAAGCCAGAAT	32	
ST147	GAACAAAGGAGAGTTGAAGGAATTGAGGAAGGTTA	35	
ST148	TCACCATCTGAGAAAGTTTTTAGAACCCTCAT	32	
ST149	CGGATTCTACCGTGTGGCTATTACGCCAGCTG	32	
ST150	AACAAAGCTAAGACTCAAGAGGCAAAAGAATA	32	
ST151	CCTGGCCCTGAAAACCACCAGA	22	
ST152	TCATTCCATAATTTAGCTTTACCCTGACTATTA	33	
ST153	AAAAACCGAAGAATAGGAACCCTAAAGGGAGC	32	
ST154	TTCGCGTCTGTTTAGTCAAAGCGCCATTCGCC	32	
ST155	AAGCGCATAAATGAAACTTATCATTCCAAGAA	32	
ST156	AAAAAGCCTGGCCTTCTCGGCCTCAGGAAGAT	32	
ST157	CCGCTTCTGGTGCCGGAGCCAGCTACGCCATCAAAAATAA	40	
ST158	TCAGAGCCGTAGCGCGGAATTTACCGTTCCAG	32	
ST159	TACAAACTCGTAACACCAAGCCCA	24	
ST160	GGCTTAATTAGATTTACTTCAAAGCGAACCAG	32	
ST161	TGCTAAACATTCAACCCGCTTTTGCGGGATCG	32	
ST162	GATTAAGAAATTCGAGGTTTGACCATTAGATA	32	
ST163	GAACGTGGATTTGAGGCCCGAACGTTATTAAT	32	
ST164	TATGCGATATATCCCAGAGGCTTTTGCAAAAG	32	
ST165	TTGGGCTTAAGTTACCCAAAGTACAACGGAGATTT	35	
ST166	TTGCCCTTGAGAGACTGTAATCAT	24	
ST167	GCGAGGCGAGGCTTATAAGTTACATCTTACCA	32	
ST168	TATGTACCTCTACAAAGCTGAAAAGGTGGCAT	32	
ST169	AAGTTTTGTTACGAGGCTGGCTCATTATACCA	32	
ST170	GAATAACATAAAAACAGGG	19	
ST171	AAAAGGAACCAGAGGGGATAAGTCCTGAACAA	32	
ST172	ACCGGAAGAAGCAAAGGCCATATTTAACAACG	32	
ST173	CTGTTTATGTTGGGAAGCAGATACATAACGCC	32	
ST174	CGCACTCCAAACCAGGATCATATGCGTTATAC	32	
ST175	TTAGCCGGCACTCATCAATACCCAAAAGAACT	32	
ST176	TCGGTTTACAACGGCTGTCACAATCAATAGAA	32	
ST177	GGCGCATCGCCTCTTCATAAATAAGGCGTTAA	32	
ST178	GGTCATAGCTGTTTCCTCGAATTCACCTTTTTAACCTCCG	40	
ST179	ATAGGAACTTCGGAACCCGTCGAGTGTAGCATTCCACAGA	40	
ST180	CCATTAGCGACAGAATCTTTTGATGATACAGG	32	
ST181	GCGGAATCGTCATAAAATTCATCAAACAACAT	32	
ST182	TATTCGGTCGCTGAGGCTT	19	
ST183	ACAAAATTATGAATATTGAAAACATAGCGATA	32	
ST184	TACCGAGCTGTGTGAAGACGGGCAACAGCTGA	32	
ST185	GAGAATAGTGGTTTACAAGACAGCATCGGAAC	32	
ST186	CTATCATAAATAGCGATCCTAATTTACGAGCA	32	
ST187	GCAAATCAACTAATAGACATTATCATTTTGCG	32	
ST188	TTAAAGGTGAATTATCACCAAACGTCACCAATGAAACC	38	
ST189	TTAGCAAAGATATTCACCAACTTTGAAAGAGG	32	

ST190	GATATAGATTTTAGCGATCCTGAAAAATCGCG	32	
1NP1	ACCCAGCTGAGCGTCTAATAGCAAGCAAATCAGTACTTCCTTAAACGACGCAGGCTTATCCTTCACGATTGCCACTTTCCAC	83	
1NP2	CCGTAATGGGGATGTGTAAATTTAATGGTTTGGTACTTCCTTAAACGACGCCTTCACGATTGCCACTTTCCAC	73	
2NP1	CAAAAGGGAATATGATAAGGCAAAGTACTTCCTTAAACGACGCCTTCACGATTGCCACTTTCCAC	65	
2NP2	CTCAAATGCTTTAAACTGCGGATGAGCTCAACGTACTTCCTTAAACGACGCCTTCACGATTGCCACTTTCCAC	73	
1NP3	GTCATTTTAGTTCAGATATAAAGTACCGACAAGTACTTCCTTAAACGACGCACTTCACGATTGCCACTTTCCAC	74	
2NP3	ACAGATGAAAATACGTATACATACATAAAGGTGTACTTCCTTAAACGACGCAGGCTTATCCTTCACGATTGCCACTTTCCAC	83	
CATCHER probe 1	TTGGGTAAATTAATTGAACCTGTCCTGCGAGCCCGGGAAGCT	42	
CATCHER probe 2	GGGAGGAAGGTCGGATCGTTTATTTCAAC	29	
PROBE	CGATCCGACCTTCCTCCCTCCTCCTCTTCCCTTGGGTCGAACATTGCTCGTCGTCACTGGGTCCTGCTCATATTGGGTTTACAGCTCACATAGGTAGACTTTAGCTTCCCGGGCTCGCAG	120	
TARGET	GGGCGGGGCGGGGGCGCGAAAGTCTACCTATGTGAGCTGTAAACCCAATATGAGCAGGACCCAGTGACGACGAGCAATGTTCGACCCAAGGGAAGAGGAGGACGCGCCCCCGCCCCGCCC	120	
SET OF STAPLES FOR 0SS TETRAHEDRON			
0ss1	TGAATCGGTGCCTAATGAGTGAGC	24	
0ss2	TAGCCCGGAGGGATAGTGAGTTTCTATGACCCTGTAATAC	40	
0ss3	GTTGTACCTATCACCGTACTCAGGAGGTTTAGCCGCCACCGAGAAGCC	48	
0ss4	CACCACCCTCATTTTCAATAGGTGAAAAACATGTCACCAG	40	
0ss5	AGTGTAAAACGACGGCTCGCAAGACAAAGAACGCGAGAAA	40	
0ss6	GTCACGACGTTGTAAAGCCTGGGGCCAACGCGCGGGGAGA	40	
SET OF STAPLES FOR 3SS TETRAHEDRON			
3ss1	TCGGTGCCTAATGAGTGAGC	20	
3ss2	TAGCCCGGAGGGATAGTGAGTTTCTATGACCCTGTA	36	
3ss3	TACCTATCACCGTACTCAGGAGGTTTAGCCGCCACCGAGAAGCC	44	
3ss4	ACCCTCATTTTCAATAGGTGAAAAACATGTCACCAG	36	
3ss5	AGTGTAAAACGACGGCTCGCAAGACAAAGAACGCGA	36	
3ss6	CGACGTTGTAAAGCCTGGGGCCAACGCGCGGGGAGA	36	

References

[S1] Alloyeau, D.;Ding, B.;Ramasse, Q.;Kisielowski, C.;Lee, Z.; Jeon, K.-J. Direct imaging and chemical analysis of unstained DNA origami performed with a transmission electron microscope. *Chemical communications* **2011**, *47*, 9375-9377.

[S2] Rafati, A.; Gill, P. Ultrastructural characterizations of DNA nanotubes using scanning tunneling and atomic force microscopes. *Journal of Microscopy and Ultrastructure* **2016**, *4*, 1-5.

[S3] Severin, N.;Dorn, M.;Kalachev, A.; Rabe, J. P. Replication of Single Macromolecules with Graphene. *Nano letters* **2011**, *11*, 2436-2439.

[S4] Moreno-Herrero, F.;Colchero, J.; Baró, A. M. DNA height in scanning force microscopy. *Ultramicroscopy* **2003**, *96*, 167-174.

[S5] Piantanida, L.;Naumenko, D.;Torelli, E.;Marini, M.;Bauer, D. M.;Fruk, L.;Firrao, G.; Lazzarino, M. Plasmon resonance tuning using DNA origami actuation. *Chem. Commun.* **2015**, *51*, 4789-4792.